VIBRATION ANALYSIS OF UNDERGROUND TUNNEL AT HIGH-TECH FACILITY

JUAN NEGREIRA MONTERO

Master's Dissertation

Structural Mechanics

VIBRATION ANALYSIS OF UNDERGROUND TUNNEL AT HIGH-TECH FACILITY

Master's Dissertation by

JUAN NEGREIRA MONTERO

Supervisor

Kent Persson, PhD,
Div. of Structural Mechanics

Examiner:

Delphine Bard, Associate Professor,
Div. of Structural Mechanics

CONTENTS

Preface

This master thesis was carried out at the Division of Structural Mechanics at LTH, Lund University, from November 2009 to May 2010.

First of all I would like to thank my supervisor PhD Kent Persson, for his continuous support, encouragement and patience. My most grateful appreciation as well to Dr. Sc. Delphine Bard for her great assistance, always motivating and helping me throughout the coarse of this work. A special thank to the staff of the Division of Structural Mechanics, the Max-Lab staff and the fellow students I shared office with for interesting and helpful discussions during meetings and coffee breaks.

I would also like to express my deepest gratitude and love to my parents Juan and Mariluz for their infinite patience, support and understanding throughout all my life. Nothing would be as it is without them.

Finally, I would like to thank all the rest of my family and friends back home (special mention to Alberto Trillo, the one always there) and all the people I met during this unforgettable year in Sweden.

Juan Negreira Montero
Lund, in May 2010.

ABSTRACT

Max-lab is a national laboratory operated jointly by the Swedish Research Council and Lund University. Nowadays, the Max project consist of three facilities (three storage rings): MAX I, MAX II, MAX III and one electron pre-accelerator called Max Injector. A new storage ring is needed due to improved nanotechnology.

MAX IV is planned to be the next generation Swedish synchrotron radiation facility. The main source at MAX IV will be a 3-GeV ring with state-of-the-art low emittance for the production of soft and hard x-rays as well as an expansion into the free electron laser field [13].

In this master thesis, the vibration levels at the Linac will be analysed. Linac stands for "Linear accelerator" and its function is to accelerate the electron beam until it has almost reached the speed of light and then shoot it into the ring where it can begin to spin around producing synchroton light. The Linac as well as the bridge over it will be mostly built on concrete, while the soil will be mainly constituted by boulder clay. Since this construction will be used for high precision measurements, it will be asked to have very strict technical conditions where only very low vibration levels will be allowed. The technical condition states that only an RMS value of 100 nm during 1 second will be permitted in the vertical direction.

Realistic finite element models of the Linac underground tunnel will be stablished in order to analyse the influence of the surrounding vibration sources on the MAX IV Lab's underground tunnel. To achieve this purpose both steady-state and transient analysis were performed:

1. In the first case, a parameter study was made by varying material properties and checking its influence on the model. Thus, the damping ratio and the density of the soil and the modulus of elasticity and the thickness of the concrete floor were varied. This was done by carrying out a frequency sweep. Likewise and since a bridge for bus traffic is supposed to be built over the Linac, a simulation of the dynamic component of a bus load was performed by means of a frequency sweep as well.

2. For the transient loads, two realistic types of loading were simulated. On one hand, an irregularity on the road was assumed and on the other hand a walking load was also performed.

All the parts in the model were meshed with solid isoparametric hexaedra elements. They are essentially constant strain elements with first-order linear interpolation. They are 8 node brick elements with no rotations, hence having only three degrees of freedom (translations) on each node. The model has a total number of 135919 nodes and 107530 elements, making a total of 407757 degrees of freedom.

In most of the cases studied, the requirement was not fulfilled, so some solutions were tried out. Thus, the addition of pillars under the bridge was checked out.

After all the simulations carried out, it can be concluded that the soil has a great influence on the response of the structure. Attention should be paid to its properties due to the lack of data existant right now. Properties could even be determined through field measurements.

Besides, the conditions of the road crossing over the bridge should periodically be checked. The analysis results indicate that the technical requirements may be reached for a bus running on smooth asphalt. However, small irregularities on the road at the bridge will create vibration levels that are too high and the quality of the measurements at the MAX IV will be affected. Since the probability of not always having a smooth road is rather high, especially during the winter, it is recommended that the bridge is avoided and that the road will be relocated to not crossing the Linac.

Likewise and looking at the simulations of the walking load, it can be concluded that worrying levels of vibrations can be caused by groups of people walking close to the beamline.

1. INTRODUCTION

1.1. Max Laboratory

Max-lab is a national laboratory operated jointly by the Swedish Research Council and Lund University. Nowadays, the Max project consists of three facilities (three storage rings): MAX I, MAX II, MAX III and one electron pre-accelerator called Max Injector, Figure 1.1.
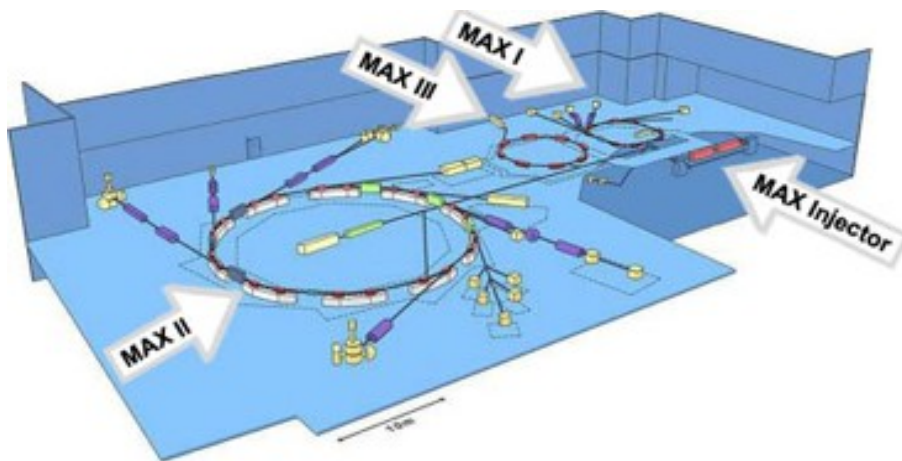
Figure 1.1: Max Laboratory.

1. MAX I: The first storage ring/pulse stretcher at Max-lab, commissioned 1986. It is used for synchrotron light production (UV and IR) and also as a pulse-stretcher for experiments in nuclear physics.

2. MAX II: This 3rd generation storage ring was commissioned 1996 and delivers synchrotron light, primarily from insertion devices, in the soft X-ray to hard X-ray spectral region. This ring is equipped with superconducting magnet structures to cover the hard X-ray spectral region.

3. MAX III: 3rd generation light source operated for production of UV light. A test-bench for novel magnet technology. Max III was commissioned 2007.

4. MAX Injector: This accelerator delivers electrons to all three storage rings as
   well as to the Free Electron Laser (FEL) experiment. The electrons from an
   RF gun are accelerated in two linear accelerator structures (linacs) and are
   then recirculated through these linacs by compact magnet structures of novel
   type [13].

1.2. MAX IV

MAX IV is planned to be the next generation Swedish synchrotron radiation facil-
ity. It will replace the existing laboratory consisting of the Max I, II and III storage
rings. The main source at MAX IV will be a 3-GeV ring with state-of-the-art low
emittance for the production of soft and hard x-rays as well as an expansion into
the free electron laser field. MAX IV will be built at Brunnshögsområdet in the
northeast of Lund [13].

A new storage ring is needed due to improved nanotechnology. As technologies de-
velop, new methods are needed in order to improve analysis of different materials.
MAX IV will be 100 times more efficient than already existing synchrotron radiation
facilities. Particles as small as a billionth of a meter can now be analysed. Therefore,
MAX IV will be a world leading facility for studies of particles at a nano-level by
using synchrotron light [13].

As shown in MAX IV's architect-drawing, Figure 1.2, [14], MAX IV consists basi-
cally of one circular-storage-main-ring and one linear underground tunnel (Linac)
next to it. Both the ring and the Linac converge at one point, where the electrons
have already almost reached the speed of light and are then shot into the ring so they
can begin to spin around. The beam is then bent with magnets in order to produce
a powerful light, synchrotron light, used in several research fields. The Linac passes
underneath the ring and continues until its end.

1.2.1. Synchrotron Light

When a charged particle moves at a relativistic speed along a curved path it emits
electromagnetic radiation which can be used as a research tool. This is the so-
called synchrotron radiation. This synchrotron radiation is artificially produced for
scientific and technical purposes by specialized particle accelerators, typically ac-
celerating electrons. The electrons are usually accelerated and then injected into a
storage ring where they begin to spin around, circulating along a curve path and
producing the synchrotron radiation. This light can be taken out at some points of
the ring and be driven towards experimental stations, where samples are placed in
the line of the radiation to be studied.

The major applications of synchrotron light are in physics, materials science, biology, environmental sciences, biomedicine, archaeology, chemistry, geology and medicine.

Figure 1.2: MAX IV

1.3. Linac

In this master thesis, the Linac will be analysed. Linac stands for *Linear Accelerator*, and its funtion is to initially accelerate the electron beam until it has almost reached the speed of light and therefore it can be shot into the ring in order to produce the synchrotron light used in the experiments performed inside the facility.

1.3.1. Geometry

The tunnel changes its cross-section shape several times along its length as shown in Figure 1.4. The Linac has a total of four different cross-section shapes.

These section changes occurs where the bridge crosses over the tunnel, the reinforcement of the tunnel due to it is passing underneath the Max-Lab II, and where it meets the MAX IV's ring.

All the sections could be obtained by extruding cuts from the most common section which looks as shown in Figure 1.3.
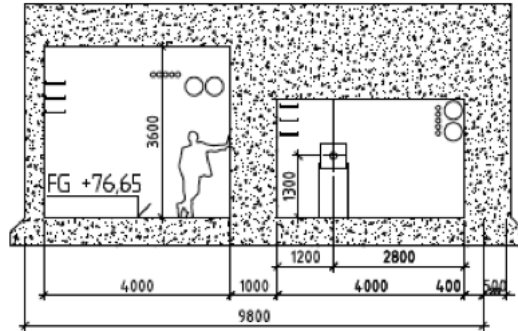

Figure 1.3: Section under the ring.

The Linac will have, as shown in Figure 1.3, two cavities. The cavity on the left is intended for installations and pedestrian traffic (hereafter denoted walking path) while the right cavity is where the electron beam will be accelerated (hereafter denoted beam path). It is indeed under this beam path where the technical requirement must be fulfilled. It is that the vibration level must be less than 100 nm (RMS value in the vertical direction during 1 s). If this requirement is not achieved, the studies performed inside the facility will not provide reliable results.

The whole variety of sections along the Linac is shown in Figure 1.4. The aim of this master thesis is to do an analysis of the vibration levels in the Linac. Since the differences between the various sections are not that big, it was assumed that the tunnel could be shaped only as a single section (Figure 1.3) extruded along its length.

In Figure 1.5, an overview of MAX IV is shown. The locations where the Linac changes its section geometry can also be seen; i.e. at the crossing underneath the Max-II hall, at where the bridge crosses over and as where it passes beneath the storage ring.

At both ends of the tunnel, there are two measurement buildings which will not be considered in the model because of their negligible influence of the vibrations near the bridge.
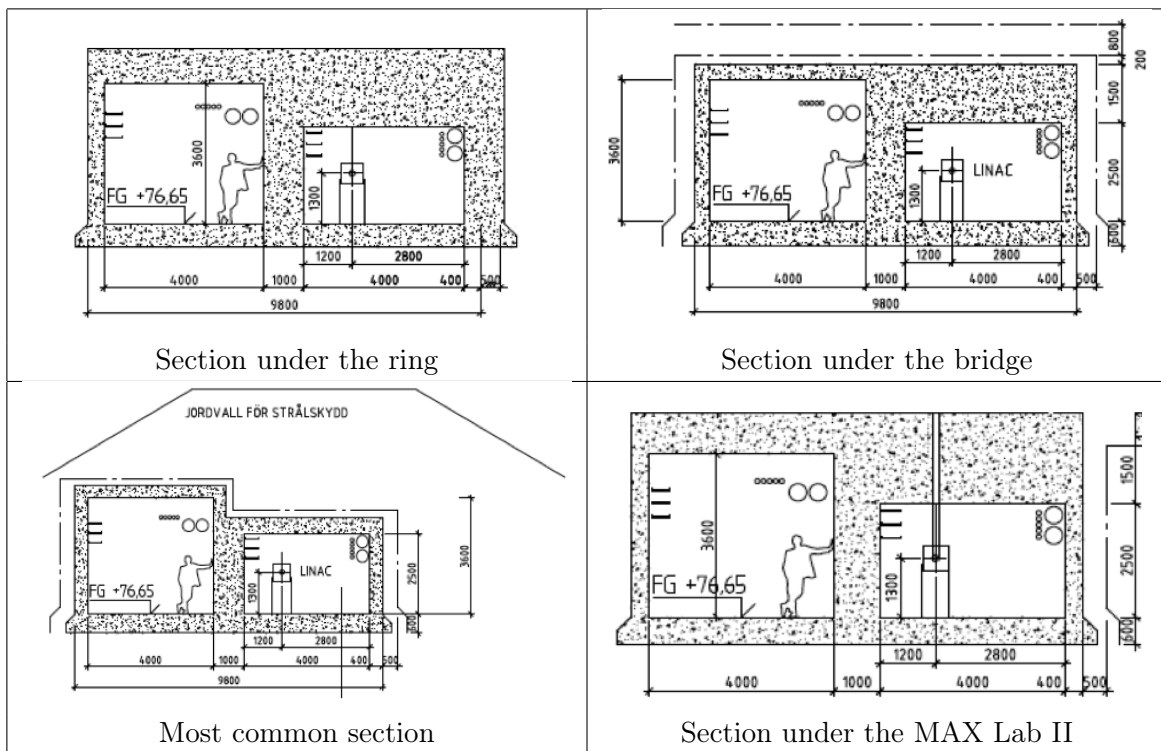
Figure 1.4: Different sections along the Linac.

The model will consist only of a single cross-section extruded along its length with the ends open. The simplifications made to the model are such that they probably will have very small influence on the validity of the results.
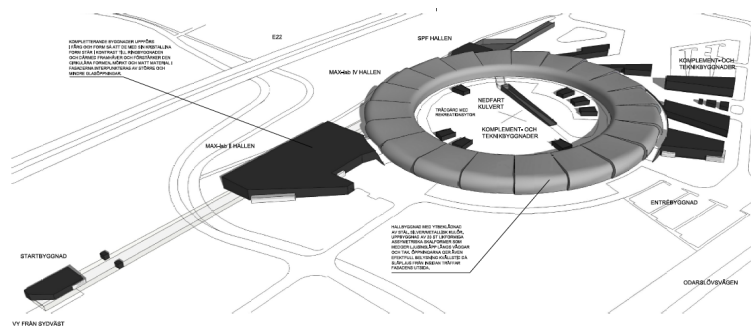

Figure 1.5: MAX IV's facilities overview.

1.4. Objective and Method

In this master thesis, the vibration levels at the Linac will be analysed. Since this construction will be used for high precision measurements, it will be asked to have very strict vibration requirement where only very low vibration levels will be allowed. The technical condition states that only an RMS value of 100 nm during 1 second will be permitted in the vertical direction.

It is obvious that the surrounding elements existing in the area will have a large influence on the Linac's behavior. Next to it there is the E22 freeway that will of course propagate waves of different frequencies, depending on the traffic intensity, towards the underground tunnel. Likewise, a bridge for bus traffic is planned to be built over the tunnel that also may disrupt the performance of the Linac's measurements.

The main aim of this master thesis is to analyse the influence of the surrounding vibration sources on the MAX IV Lab's underground tunnel by means of the finite element method. Realistic finite element models of the Linac underground tunnel must be stablished in order to analyse this influence. Likewise, it will be necessary to model with different assumptions loads, materials, etc. in order to prove the fulfillment of the needed requirement. If the vibration requirement is not fulfilled for the proposed structure, solutions to meet it could be pointed out as well.

1.5. Disposition

This report is divided in the following chapters:

1. Chapter 2 contains an introduction of vibration theory.

2. Chapter 3 describes the materials presented in the model.

3. Chapter 4 introduces the finite element method and its formulation.

4. Chapter 5 deals with the FE model employed in this study.

5. Chapter 6 presents all the modelling results

6. Chapter 7 contains a discussion of the investigation made.

7. Chapter 8 suggest several options for further work.

8. In the Appendix, all plots as well as Matlab codes used are presented.

2. Structural Dynamics. Vibration Theory

2.1. Introduction

Vibrations appear in uncountable situations in daily life, either in machines as well in structures, etc. It would be impossible to make a list of all this situations. These vibrations normally appear in systems subjected to the action of forces depending on time. Thus, structural dynamics describes the behavior of a structure due to dynamic loads.

We can consider a vibration, in its easiest form, as the oscillation or the repetitive movement of an object around an equilibrium position. This equilibrium position is the one the object would tend to return to when the force over it is zero [11].

Dynamic loads are applied to structures as a function of time resulting in time-varying responses. Therefore, vibrations can be described and measured as displacements (distance from a reference or equilibrium point), as velocities or as accelerations. A vibration signal can be described in the time domain (acceleration plotted versus time, Figure 2.1a), or in frequency domain (acceleration plotted versus frequency, Figure 2.1b). This last way of plotting a vibration signal is called response spectrum. Fourier analysis methods such as FFT (Fast Fourier Transform) can easily make the leap between domains.

When analyzing structures subjected to time dependent loading, the method of analysis is completely different from the one used in the static case. While doing conventional structure analysis, a structure subjected to static loads can be solved with classical methods (even an expert engineer could provide at first sight solutions similar to the real ones). In the static case it can be said that the solution follows the natural intuition: *the more load you have, the more section you need.* However, when vibrations come to scene, the situation radically changes. Then, the magnitude of the force may not be that important as its frequency. Intuition can now lead us to fatal errors since small periodic loads can, for instance, be much worse than greater static forces [5].
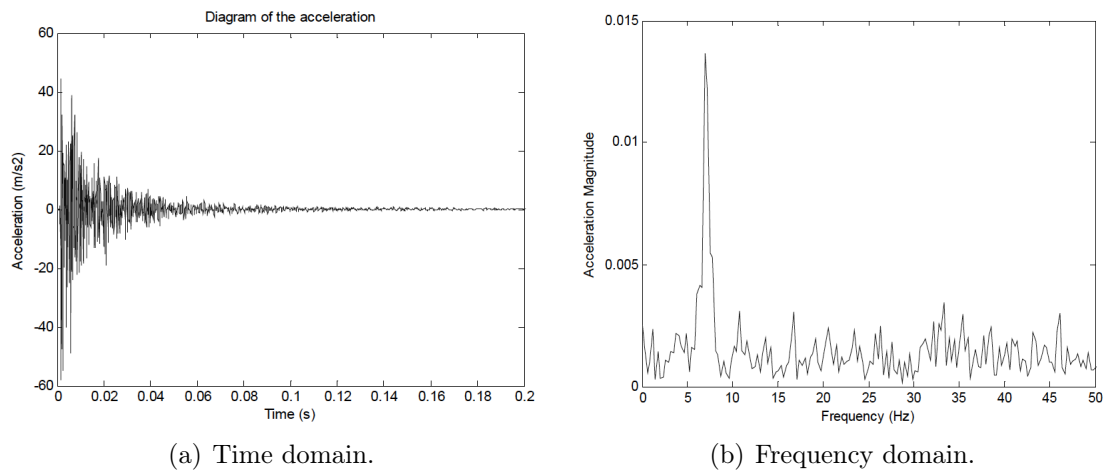
(a) Time domain.   (b) Frequency domain.

Figure 2.1: Example of plotting result in different domains

2.2. Single-Degree-of-Freedom (SDOF) Systems

We define the degrees of freedom (DOF) of a system as the number of independent displacements required to define the exact position of it. Thus, we can distinguish between discrete systems (where a finite number of DOF is needed) or continuous systems (when we need an infinite number of DOF to define it completely).

Mathematically, discrete systems lead to a system of ordinary differential equations, while continuous lead to a system of differential equations with partial derivatives. Continuous problems are very hard to solve by analytic methods, and they are normally discretized and solved by using Finite Element Method (FEM) techniques.

Only one DOF is needed to describe the behavior of a single-degree-of-freedom system. The classic SDOF system is a mass-spring-damper system, considering the spring and the damper to be massless, the mass as a lumped mass and all the motions in the direction of the x-axis as shown in Figure 2.2.
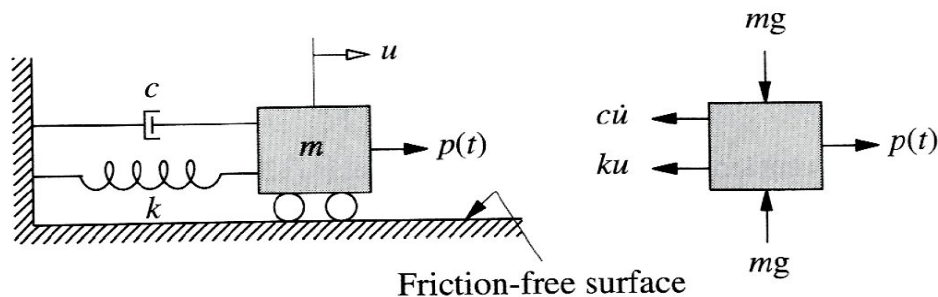

Figure 2.2: Mass-spring-damper SDOF system.

As seen in Figure 2.2, the external force is acting in the positive direction of the x-axis, while the resistant elastic and damping forces are in the opposite direction. It is possible to find the response of this SDOF system by solving the force equilibrium given by the Newton's second law of motion equation.

$$p(t) - f_s - f_d = m\ddot{u} \tag{2.1}$$

where

$f_s = ku$ is the elastic force
$f_d = c\dot{u}$ is the damping force (related with the velocity of the structure)
c: viscous damping coefficient [Ns/m]
$p(t)$ is the external force applied (depending on time)
$f_I = m\ddot{u}$ is the inertial force of the mass

Rearranging terms:

$$m\ddot{u} + c\dot{u} + ku = p(t) \tag{2.2}$$

wich is the differential equation describing the motion of the system.

The displacements of the system, $u(t)$, can easily be obtained by solving Eq. 2.2.

2.3. Multi-Degree-of-Freedom (MDOF) Systems

A structure normally has an infinite number of degrees of freedom. However, it is possible to create an approximate model of it with a finite number of DOF by considering a finite number of massless elements and a finite number of node displacements (the mass is lumped on these nodes). It is the so-called MDOF system.

It is easy to demonstrate from the same example as the SDOF systems previously analysed that the linear equations of motion in an N-degree-of-freedom discrete system subjected to small displacements in generalized coordinates can be written as Eq.2.3.

$$\mathbf{M\ddot{u}} + \mathbf{C\dot{u}} + \mathbf{Ku} = \mathbf{p}(t) \tag{2.3}$$

where

N is the number of degrees of freedom
$\mathbf{M}(N \times N)$ is the mass matrix; symmetric and positive-definite
$\mathbf{C}(N \times N)$ is the damping matrix

$\mathbf{K}(N \times N)$ is the stiffness matrix symmetric and whether positive or semi positive-definite

$\mathbf{p}(t)$ is the external load vector which contains the dynamic external forces. Its dimension is $(N \times 1)$

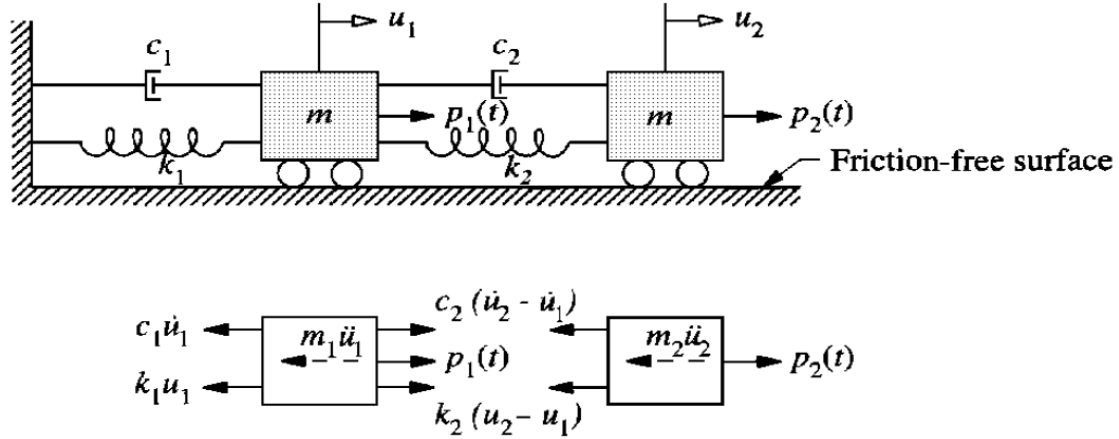$\mathbf{u}(t)$ is the vector of displacements with dimension $(N \times 1)$.

Figure 2.3: Two DOF system: Mass-spring-damper MDOF system.

2.4. Modal Analysis

Modal analysis can be used to determine natural frequencies and the vibration mode shapes of a structure. Taking Eq.2.3 and particularizing it for the free vibration case ($\mathbf{p} = \mathbf{0}$) in a non-damped system ($\mathbf{C} = \mathbf{0}$), it leads to:

$$\mathbf{M\ddot{u}} + \mathbf{Ku} = \mathbf{0} \tag{2.4}$$

with the initial conditions $\mathbf{u}(0) = \mathbf{u}_0$ and $\dot{\mathbf{u}}(0) = \dot{\mathbf{u}}_0$

We assume a harmonic solution as follows:

$$\mathbf{u}(t) = \mathbf{A}e^{st} \tag{2.5}$$

where $\mathbf{A}$ is an amplitude vector and s are the different square roots of the eigenvalues of the problem.

Substituting 2.5 in 2.4 it leads to:

$$(s^2\mathbf{M} + \mathbf{K})\mathbf{A}e^{st} = \mathbf{0} \tag{2.6}$$

Nor e^{st} either $\mathbf{A}$ can be 0 (trivial solution), so:

$$(s^2\mathbf{M} + \mathbf{K})\mathbf{A} = \mathbf{0} \tag{2.7}$$

2.4.1. Natural Frequencies

In order to calculate the values of $\mathbf{A}$ and s, it is necessary to solve Eq.2.7, which is an eigenvector and eigenvalue problem. Obviously, this problem has a solution different from the trivial one if and only if the coefficient matrix is singular, i.e. if its determinant is zero.

$$|s^2\mathbf{M} + \mathbf{K}| = \mathbf{0} \tag{2.8}$$

It is possible to demonstrate that if $\mathbf{M}$ is positive-definite and $\mathbf{K}$ is positive or semi positive-definite, all the eigenvalues s^2 are real and negative or zero.

In order to just considering positive values, it is appropriate to make the following change of variable:

$$s^2 = -\omega^2 \Rightarrow s = \pm\omega i \tag{2.9}$$

and substituting 2.9 in 2.10 leads to:

$$|\mathbf{K} - \omega^2\mathbf{M}| = 0 \tag{2.10}$$

with the eigenvalues $\omega_1^2, \omega_2^2, ..., \omega_n^2$ positives or zero; whose square roots are the so-called natural frequencies of the system.

When a structure is disturbed from its static equilibrium position and is allowed to oscillate without any external dynamic excitation, it will vibrate with certain frequencies. Those frequencies are the above calculated values. A structure has an unlimited number of natural frequencies, which are a property of the structure and in principle they depend on the mass, the distribution of mass and the stiffness of the structure [5].

The vibration mode shapes of a structure are deformed shapes of the structure at a specified frequency as it will be explained afterwards.

If the finite element method is used to model the structure it will have as many natural frequencies and corresponding mode shapes as there are degrees of freedom. The natural frequencies of a damped system differ somewhat from the natural frequencies of the same system without damping. However, for lightly damped structures with damping ratios below 20 %, the natural frequencies of damped vibrations are approximately the same as the natural frequencies of the structure without damping [1].

2.4.2. Resonance

If a structure is subjected to a dynamic force whose frequency is close to one of its natural frequencies, the response can be strongly enhanced, increasing its amplitude. Both the amplitude and the acceleration will become very high. This phenomenon is the so-called resonance. Without the presence of any damping, this amplitude will gradually grow tending to infinite. However, some damping is always present in structures (joints, micro-cracks...) preventing from this crescent and uncontrolled oscillations [1].

Figure 2.4 represents the effects of some damping ratios on the resonant response. The deformation response factor (Rd) on the y-axis is the ratio of the dynamic deformation to the static deformation while the x-axis shows the ratio between the current frequency and the natural frequency [1].
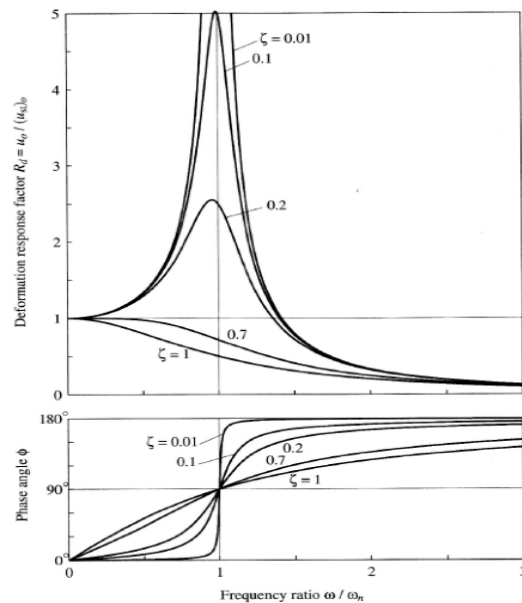

Figure 2.4: Deformation response factor for a damped system excited by a harmonic force.

2.4.3. Vibration Modes

Associated with every eigenvalue ω_i^2 there is a N-dimension eigenvector which can be obtained from Eq.2.11.

$$(\mathbf{K} - \omega_i^2\mathbf{M})\mathbf{A}_i = 0 \tag{2.11}$$

This system of equations is homogeneous and its coefficient matrix is singular. Hence, it has a solution different from the trivial zero. This eigenvectors receive the name of vibration modes.

It is possible to write the general solution for free vibration as a linear combination of the calculated solutions given by Eq.2.5 as follows:

$$u(t) = \mathbf{A}_1(\beta_{1_1}e^{i\omega_1 t} + \beta_{1_2}e^{-i\omega_1 t}) + ... + \mathbf{A}_N(\beta_{N_1}e^{i\omega_N t} + \beta_{N_2}e^{-i\omega_N t}) \tag{2.12}$$

where the constants β_i can be obtained from the initial conditions.

Likewise, the previous equation can also be written as a combination of harmonic simple functions.

$$u(t) = \mathbf{B}_1\mathbf{A}_1 cos(\omega_1 t - \psi_1) + ... + \mathbf{B}_N\mathbf{A}_N cos(\omega_N t - \psi_N) \tag{2.13}$$

where, again, the constants B_i and ψ_i can be calculated with the initial conditions.

It is easy to see in Eq.2.13 that the free vibration response can be written as a linear combination of the modes of vibration. Each coefficient is given by a time lagged harmonic function whose vibration frequency is, indeed, the frequency correspondent to that mode of vibration.

2.5. Damping

Damping is, in general terms, the reduction of a vibration response. It is always present in structures in many ways: friction in joints, internal properties of materials, contract zones, opening and closing micro-cracks in the concrete, etc. It has a large influence on the response of a structure loaded dynamically [1].

Nowadays, there is a lack of knowledge of the actual physical phenomena and mechanisms which cause damping due to the fact that these properties of materials are not well established. Therefore, Rayleigh damping was used in the model of the Linac underground tunnel. In this kind of damping, it is considered that the damping matrix is a linear combination of the mass matrix and the stiffness matrix according to Eq.2.14.

$$\mathbf{C} = a_o \mathbf{M} + a_1 \mathbf{K} \tag{2.14}$$

where the damping ratio for the nth-mode is given by Eq.2.15.

$$\zeta_n = \frac{a_0}{2}\frac{1}{\omega_n} + \frac{a_1}{2}\omega_n \tag{2.15}$$

This damping ratio is proved not to be constant for all modes of vibration. a_0 and a_1 are constants based on the damping of two natural frequencies of the structure.

$$a_0 = \zeta\frac{2\omega_i\omega_j}{\omega_i + \omega_j} \tag{2.16}$$

$$a_1 = \zeta\frac{2}{\omega_i + \omega_j} \tag{2.17}$$

In applying this procedure to a practical problem, i and j with specified damping ratios should be chosen to ensure reasonable values for the damping ratios in all the modes contributing significantly to the response [1].

Although the assumption that the damping is proportional to the mass and stiffness matrices has no rigorous physical basis, it leads to reasonable results. Besides, in practice, the damping distribution is rarely known in sufficient detail to warrant any other more complicated model [8].

In general, it is more important to damp the lower frequencies. As stated by the formula, a_0 is more important for lower modes, while a_1 is mostly important for the higher frequencies (i.e. the lower frequencies are damped with the mass of the system and the damping forces depend on the absolute velocities of the model; while the higher frequencies are damped with the stiffness and the damping is proportional to the strain rate).
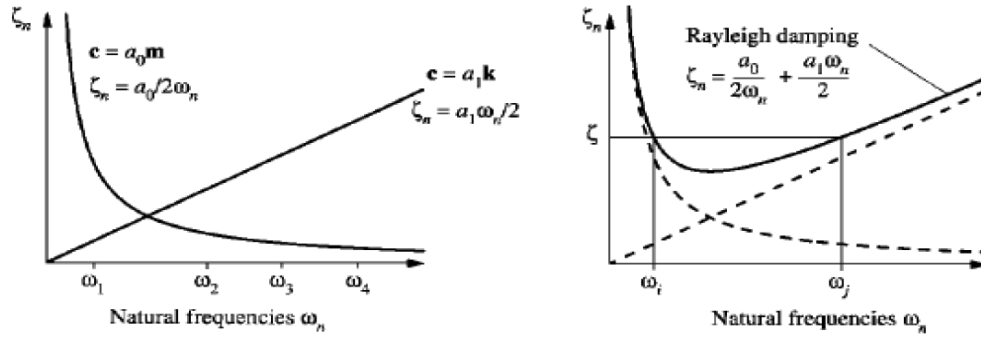
Figure 2.5: (a) Mass damping and Stiffness damping (b) Rayleigh damping.

2.5.1. Damping Ratio

It is common, as seen above, to use the damping ratio ζ instead of the damping constant c. This ratio ζ is a dimensionless measure of damping. It shows the ratio of the actual damping in the structure, in terms of the damping constant c, to the critical damping coefficient c_{cr}. This critical damping coefficient is the smallest value of c that makes the system return to its equilibrium position without oscillating.

Therefore, it is possible to make a classification attending to this damping ratio [1]:

1. Underdamped system: $c < c_{cr} \Rightarrow \zeta < 1$

2. Critically damped system: $c = c_{cr} \Rightarrow \zeta = 1$

3. Overdamped system: $c > c_{cr} \Rightarrow \zeta > 1$

where c responds to the following formula:

$$\zeta = \frac{c}{c_{cr}} = \frac{c}{2\sqrt{km}} \tag{2.18}$$

ζ: damping ratio
c: viscous damping coefficient
c_{cr}: critical damping coefficient
k: stiffness of the system
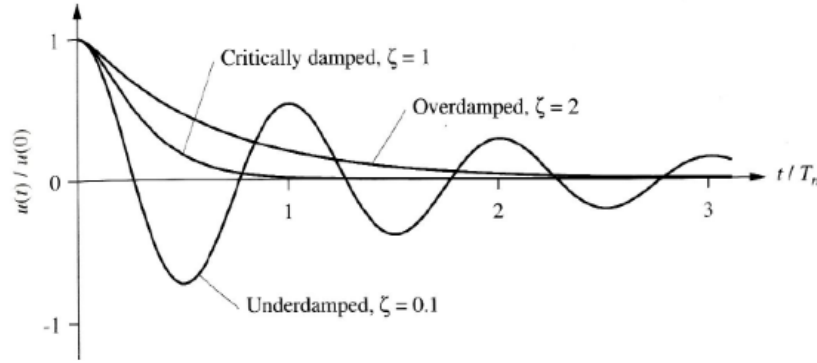m: mass of the system.

Figure 2.6: Free vibration of critically damped, underdamped and overdamped systems.

2.6. RMS Value

RMS is the abreviation of root mean square (also known as the quadratic mean). It is a statistical measure suitable or applicable to a varying magnitude since it gives back an "efficient average value" of it even though the magnitude is constantly changing.

The technical requirement MAX IV has is expressed in terms of RMS value. The technical condition states that only an RMS value of 100 nm during 1 second will be permitted in the vertical direction.

The RMS value of the vertical displacement responds to Eq.2.19.

$$u_{RMS} = \sqrt{\frac{1}{\Delta t} \int_{t_0}^{t_0+\Delta t} u^2(t)\, dt} \qquad (2.19)$$

2.7. Wave Length

The wave length of the waves travelling through the structure has a large influence on the model, since it will determine the size of the elements when meshing the model as it will be explained afterwards.

The bending wave number for an isotropic plate is given by Eq.2.20, [20].

$$k = \sqrt[4]{\frac{\omega^2 \rho h}{EI}} \qquad (2.20)$$

where ρ is the density of the plate, ω the angular frequency, h the height of the plate and EI is the bending stiffness of the cross-section.

The bending wave number can be calculated with Eq.2.21.

$$k = \frac{2\pi}{\omega} = \frac{\omega}{c} \tag{2.21}$$

Introducing Eq.2.21 in 2.20, it leads to Eq.2.22.

$$c = \sqrt{\omega}\sqrt[4]{\frac{EI}{\rho h}} \tag{2.22}$$

wich is the expression giving the bending wave speed in an isotropic plate.

The wave length is defined as the ratio between the wave speed and the frequency.

$$\lambda = \frac{c}{f} \tag{2.23}$$

The wave speed for a shear and a surface wave are respectively given by Eq.2.24 and 2.25.

$$c = \sqrt{\frac{G}{\rho}} \tag{2.24}$$

$$c = \sqrt{\frac{E}{\rho}} \tag{2.25}$$

Shear waves or also transverse waves appear in a elastic medium when subjected to periodic shear. The disturbance is an elastic deformation (change of shape with no change of volume) perpendicular to the direction of motion of the wave.

Surface waves are waves travelling along a material surface with both transverse and longitudinal motion involved. The particles in a solid, through which a Rayleigh surface wave passes, move in elliptical paths.

3. Materials

3.1. Boulder Clay

Whenever a glacier or ice-sheet has retreated from an area, it leaves behind its characteristic deposits of sediments (*glacial drift*). More than one-third of the Earth was glaciated during the Pleistocene and a greater area was covered by glacial drift [15]. Boulder clay is defined as a deposit of clay, often full of boulders, which is formed in and beneath glaciers and ice-sheets wherever they are found, but is in a special sense the typical deposit of the Glacial Period in northern Europe and America [19]. It is deposited as an irregular layer over the surface of the ground and it is unstratified unless where modified by water. The colour of the clay derives from that of the rocks from which the ice obtained raw material during its passage (it is the result of the direct or indirect abrasion of the older rocks), [15].

Boulder clays may be quite problematic in construction due to their extreme variability. They may consist of a high proportion of stones and boulders or may be nearly entirely of clay. They can even mask the true nature of the underlying rock surface, concealling hollows. Properties of boulder clay depend of how the ice has packed it [15].

Boulder clays are usually water-saturated, wich makes them have a Poisson's ratio of 0.5 since the water is incompressible. The density for a clay normally varies from 1400 to 2000 kg/m^3. Boulder clay's density should be closer to 2000 kg/m^3 due to its coarse graded disposition. Its damping ratio is strain dependent, being able to oscillate from 1% to 20% and increasing with the strain. Furthermore, its value is different for each load magnitude and case. Boulder clay's undrained shear strength may be 200-300 kPa, [18].

3.2. Concrete

Concrete is a construction material. It is composed of cement and other cementitious materials such as fly ash and slag cement, aggregate (generally a coarse aggregate such as gravel, limestone, or granite, plus a fine aggregate such as sand), water, and chemical admixtures. When concrete is mixed with water, it solidifies and hardens due to a chemical process. This process is the so-called hydration.

Concrete is used more than any other man-made material in the world (in pavements, architectural structures, foundations, roads, bridges, etc). According to the swedish building authority *Boverket*, it has a density of 2400 kg/m^3, and the Poisson ratio is 0.2. *Boverket* also classifies different types of concrete concerning compressive stress (5% fractile of the statistical distribution). Thus, for static analysis, different types of concrete whose Young's modulus varies from 27 to 39 GPa can be chosen. For dynamic loading, *Boverket* advices to use a multiplication factor of 1.2 for the modulus of elasticity. The damping ratio for concrete varies between 2% and 10%, where the higher number is for heavily cracked concrete, [1].

The main structural characteristic of the concrete is that it withstands very well compression strains while its behavior under other types of strains (tensile, torsion and shear) turns to be weak. Due to this reason, concrete is normally used reinforced with steal. Hence, reinforced concrete and prestressed concrete are the most widely used modern kinds of concrete, whose main characteristics are:

1. Reinforced concrete: In this type of concrete, some reinforcement bars ("rebars"), grids, plates or fibers are introduced to strengthen the concrete in tension. The reinforcement also has the mission of holding the cracked sections together.

2. Prestressed concrete: with this technique it is also possible to overcome the concrete's natural weakness in tension. In this method, tendons inside poured concrete (normally high tensile steel cable or rods) are used to introduce deliberately previous compressive stresses in the concrete. Like this, it offsets the tensile stress the concrete would otherwise experience under a bending load (i.e. with a prestressed concrete, when subjecting it to a tensile strain, the force would first have to dis-compress the concrete so the admitted load would be greater). It can be used to produce beams, floors or bridges with a longer span.

4. Finite Element Method (FEM)

4.1. Introduction

Finite Element Method (hereafter FEM) was used to perform the vibration analysis of the Linac tunnel at MAX IV.

Engineering problems are all modelled by differential equations which can be nearly impossible to solve by classical analytical methods. The Finite Element Method is a numerical approach by which boundary value differential equations can be solved in an approximate manner.

The differential equation, or equations, describing the physical problem considered, is assumed to hold over a certain region (1D, 2D or 3D regions). The region is then divided into smaller parts (finite elements), and then usually a polynomial approximation over the element is made. The collection of all elements is called a finite element mesh. The correct choice of element for a particular simulation is vital if accurate results are to be obtained at a reasonable cost. Having determined the behavior of the elements, they are assembled together, using some specific rules, to form the entire region, which eventually enables us to obtain an approximate solution for the behavior of the entire body, [2].

As the FE method is a numerical mean of solving general differential equations, it can be applied to various physical phenomena. In this master thesis, a realistic finite element model of the Linac underground tunnel will be stablished in order to predict the vibrations in it with high accuracy.

4.2. Isoparametric Finite Elements

Normally, the sides of quadrilateral and brick elements must be parallel to the coordinate axes in order to behave in a compatible manner. This restriction is very difficult to fulfill when modelling bodies with arbitrary geometries. However, it can be done with isoparametric elements.

Consider a cubic domain bounded in a $\xi\eta\zeta$-coordinate system (parent domain) and bounded by $\xi = \pm 1$, $\eta = \pm 1$ and $\zeta = \pm 1$. The transformation through which the parent domain is transformed into another more complicated region is called

29

mapping. The *mapping* transforms the parental domain into a global Cartesian *xyz*-coordinate system as follows:

$$x = x(\xi, \eta, \zeta); \qquad y = y(\xi, \eta, \zeta); \qquad z = z(\xi, \eta, \zeta); \tag{4.1}$$

This relation is univocal, i.e. for every point given by its $\xi\eta\zeta$-coordinates in the parent domain, there exists a unique point given by its *xyz*-coordinates in the global domain.
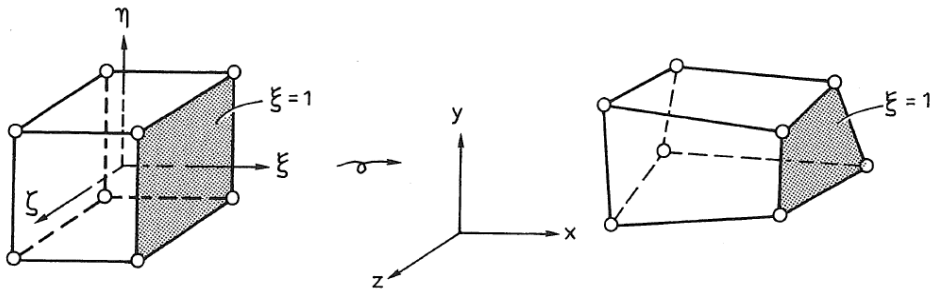

Figure 4.1: Eight-node three-dimensional isoparametric element.

Differentiating Eq.4.1 and using the chain rule, it leads to the expression which allows the transformation between two domains:

$$\begin{bmatrix} dx \\ dy \\ dz \end{bmatrix} = \begin{bmatrix} \frac{\partial x}{\partial \xi} & \frac{\partial x}{\partial \eta} & \frac{\partial x}{\partial \zeta} \\ \frac{\partial y}{\partial \xi} & \frac{\partial y}{\partial \eta} & \frac{\partial x}{\partial \zeta} \\ \frac{\partial z}{\partial \xi} & \frac{\partial z}{\partial \eta} & \frac{\partial z}{\partial \zeta} \end{bmatrix} \begin{bmatrix} d\xi \\ d\eta \\ d\zeta \end{bmatrix} \tag{4.2}$$

The matrix $\mathbf{J}$ is related to the *mapping* and is called the *Jacobian matrix.*

$$\mathbf{J} = \begin{bmatrix} \frac{\partial x}{\partial \xi} & \frac{\partial x}{\partial \eta} & \frac{\partial x}{\partial \zeta} \\ \frac{\partial y}{\partial \xi} & \frac{\partial y}{\partial \eta} & \frac{\partial x}{\partial \zeta} \\ \frac{\partial z}{\partial \xi} & \frac{\partial z}{\partial \eta} & \frac{\partial z}{\partial \zeta} \end{bmatrix} \tag{4.3}$$

If the values in the parental domain are the ones to be determined given dx and dy, it follows that:

$$\begin{bmatrix} dx \\ dy \\ dz \end{bmatrix} = \mathbf{J}^{-1} \begin{bmatrix} d\xi \\ d\eta \\ d\zeta \end{bmatrix} \tag{4.4}$$

which obviously requires det $\mathbf{J} \neq 0$

It is emphasized that, even when the mapping is unique, this does not necessarily imply that it is possible to invert 4.1 and obtain explicit solutions in the form $\xi = \xi(x, y, z)$, $\eta = \eta(x, y, z)$ and $\zeta = \zeta(x, y, z)$.

If an element behaves in a conforming, i.e. compatible manner in the parent domain, its isoparametric version also behaves in a conforming way and no mismatch between adjacent elements exists. The completeness criterion will be satisfied if and only if:

$$\sum_{i=1}^{n} \mathbf{N}_i^e = 1 \tag{4.5}$$

If the compatibility and completeness requirements are fulfilled individually, then the element fulfills the convergence criterion as well.

When mapping an element, it requires that the vertex-nodes on the parent domain also must be located in the boundary after the transformation, [2].

4.3. Finite Element Formulation of 3D-Elasticity

Fot three-dimensional problems, the differential equations of equilibrium are given by Eq.4.6, [3].

$$\sigma_{ji,j} + b_i = \rho \ddot{u}_i \qquad i, j = 1, 2, 3 \tag{4.6}$$

where σ_{ij} are the stress components, ρ is the mass density, b_i the body force components and $(\cdot)$ denotes the partial differentiation with respect to time.

Note also that $\sigma_{ij} = \sigma_{ji}$.

Eq.4.6 holds at all the points x_i in the domain of the problem Ω. Stress boundary conditions are given by the stress boundary condition 4.7 for all the points which lie in the part of the boundary denoted Γ_t.

$$t_i = \sigma_{ji} n_j = \bar{t}_i = \begin{bmatrix} t_x \\ t_y \\ t_z \end{bmatrix} = \begin{bmatrix} \sigma_{xx} n_x + \sigma_{xy} n_y + \sigma_{xz} n_z \\ \sigma_{yx} n_x + \sigma_{yy} n_y + \sigma_{yz} n_z \\ \sigma_{zx} n_x + \sigma_{zy} n_y + \sigma_{zz} n_z \end{bmatrix} \tag{4.7}$$

The "strong form" of the equilibrium equations holds for every single point in the domain, but when it comes to work with the finite element method, the domain

must be discretized, and so the solution of the strong form. A variational (weak) form of the equilibrium equations may be written by applying procedures as the Green-Gauss theorem to the "strong form" and therefore it yields the virtual work equations given by 4.8.

$$\int_{\Omega} \delta \mathbf{u}^T \rho \ddot{\mathbf{u}} d\Omega + \int_{\Omega} \delta \varepsilon^T \sigma d\Omega - \int_{\Omega} \delta \mathbf{u}^T \mathbf{b} d\Omega - \int_{\Gamma} \delta \mathbf{u}^T \bar{\mathbf{t}}_i d\Gamma = 0 \qquad (4.8)$$

Finite element approximations to displacements and virtual displacements are denoted by

$$\mathbf{u}(\mathbf{x}, t) = \mathbf{N}(\mathbf{x}) \tilde{\mathbf{u}}(t) \qquad \delta \mathbf{u}(\mathbf{x}) = \mathbf{N}(\mathbf{x}) \delta \tilde{\mathbf{u}} \qquad (4.9)$$

or in isoparametric form as

$$\mathbf{u}(\xi, t) = \mathbf{N}(\xi) \tilde{\mathbf{u}}(t) \qquad \delta \mathbf{u}(\xi) = \mathbf{N}(\xi) \delta \tilde{\mathbf{u}} \quad with \quad \mathbf{x}(\xi) = \mathbf{N}(\xi) \tilde{\mathbf{x}} \qquad (4.10)$$

and may be used to compute virtual strains as

$$\delta \varepsilon = \mathbf{S} \delta \mathbf{u} = (\mathbf{S} \mathbf{N}) \delta \tilde{\mathbf{u}} = \mathbf{B} \delta \tilde{\mathbf{u}} \qquad (4.11)$$

in which the three-dimensional strain-displacement matrix is given by

$$\mathbf{B} = \begin{bmatrix} N_{,1} & 0 & 0 \\ 0 & N_{,2} & 0 \\ 0 & 0 & N_{,3} \\ N_{,2} & N_{,1} & 0 \\ 0 & N_{,3} & N_{,2} \\ N_{,3} & 0 & N_{,1} \end{bmatrix} \qquad (4.12)$$

In the above, $\tilde{\mathbf{u}}$ denotes time-dependent nodal displacement parameters and $\delta \mathbf{u}$ represents arbitrary virtual displacement parameters, while $\mathbf{N}_{,i}$ is the global shape function.

Noting that the virtual parameters $\delta \mathbf{u}$ are arbitrary it can be obtained a expression for the discrete problem

$$\mathbf{M} \ddot{\tilde{\mathbf{u}}} + \mathbf{C} \dot{\tilde{\mathbf{u}}} + \mathbf{P}(\sigma) = \mathbf{f} \qquad (4.13)$$

where

$$\mathbf{M} = \int_\Omega \mathbf{N}^T \rho \mathbf{N} d\Omega \tag{4.14}$$

$$\mathbf{f} = \int_\Omega \mathbf{N}^T b \, d\Omega + \int_{\Gamma_t} \mathbf{N}^T \bar{\mathbf{t}}_i d\Gamma \tag{4.15}$$

$$\mathbf{C} = \int_\Omega \mathbf{N}^T \mu \mathbf{N} d\Omega \tag{4.16}$$

$$\mathbf{P}(\sigma) = \int_\Omega \mathbf{B}^T \sigma d\Omega \tag{4.17}$$

The term $\mathbf{P}$ is often referred to as the *stress divergence* or *stress force* term.
In the case of linear elasticity the stress is inmediatly given by the stress-strain constitutive relation

$$\sigma = \mathbf{D}\varepsilon \tag{4.18}$$

$\mathbf{D}$ is normally an elastic moduli written in a matrix form, [3].

5. FE Model

5.1. Software: Abaqus

The software used to carry out all the calculations in this master thesis was Abaqus. This software is a package for finite element analysis created by Dassault Systems. It has three different parts: Abaqus/CAE, Abaqus/Standard and Abaqus/Explicit.

The model was created in the Abaqus/CAE environment, a graphical user interface for modeling, meshing and post-processing and then calculated afterwards in Abaqus/Standard, suitable for finite element problems such as static, low-speed or steady-state dynamic analyses. The Abaqus/Explicit environment is more useful for high-speed, non-linear and transient analyses, [8].

This software is used in a wide range of fields such as automotive, aerospace, mechanics, etc.

5.2. Geometry

As it was previously explained in chapter 1, as the tunnel goes by, it changes its cross-section several times. Since the differences between them are not very significant, the model will only consist in a unique cross-section extruded along the length of the Linac with its ends open. The results obtained with these assumptions will be valid for the analysis since the simplifications introduced were judged to have a small influence on the results.

5.3. Materials

Both the soil and the concrete were modelled as linear elastic isotropic materials. The properties chosen for the two materials are given below.

5.3.1. Concrete

The Linac and the bridge over it will be built completely by concrete, considering only slightly cracked concrete. The properties used for the concrete were: density of 2400 Kg/m^3 and a modulus of elasticity of 40 GPa, properties corresponding to

the type of concrete C32/40 according to the Swedish building authority *Boverket* (with the dynamic addition, i.e. a multiplication factor of 1.2, already taken into account). The Poisson's ratio of the concrete was set to 0.2 and the damping ratio to 2%. In Table 5.1 the properties of the concrete used in the calculations are shown.

Table 5.1: Properties of the concrete

E [GPa]	ρ [Kg/m^3]	ν	ζ [%]
40	2400	0.2	2

Note that these are the base set of parameters. Further on they will be varied to determine their influence on the vibration levels.

5.3.2. Soil

The modulus of elasticity of the soil, according with the MAX IV geotechnical report [13] follows the formula:

$$E(z) = 22 + 5z \qquad \text{[MPa]} \qquad (5.1)$$

where z is the soil depth in m.

To represent that the E varies with the depth, the soil was divided in 8 different equally thick 1.2 m layers, each one of them taking the corresponding modulus of elasticity of the middle point in each layer. The Poisson ratio was set to 0.45, the density was considered to have the constant value of 1800 Kg/m^3 and the damping ratio was set for the base set to 20%. The damping ratio is strain dependent and varies for the load magnitude. Table 5.2 shows the base set of properties of the soil.

Table 5.2: Different layers of the soil

Layer	z [m]	E[MPa]	ρ [Kg/m^3]	ν	ζ [%]
1	0.6	25	1800	0.45	20
2	1.8	31	1800	0.45	20
3	3	37	1800	0.45	20
4	4.2	43	1800	0.45	20
5	5.4	49	1800	0.45	20
6	6.6	55	1800	0.45	20
7	7.8	61	1800	0.45	20
8	9	67	1800	0.45	20

A fact regarding the lack of knowledge about the properties of the soil was a big inconvenienient when performing this study. Therefore, these values were varied to check their influence on the vibration levels in the "Parameter study" section which will be discussed further on.

Note that the Linac will have earth over it as shown in the drawings, [13]. This earth will have the same characteristics as the soil on the surface; i.e. $z = 0.6$ m and $E = 25$ MPa. To perform the calculations in the worst possible case, this ground was avoided in the model. Thus, the soil was modelled along the Linac's edges and further down to 9.6 m with a width of 50 m.

5.4. Simplified Model

Linac's total length is 385 meters. At the first modelling attempt with a point load in the middle of the walking path, it was noticed that the calculation time was too long. Therefore, a simplified model was needed in order to avoid long computation times in subsequent calculations.

Reducing the length of the underground tunnel to just studying half of it was first tried with success as shown below. If the technical specifications were fulfilled at the end of a *half-length* tunnel (i.e. 192.5 meters), they would be of course fulfilled at the end of the *full-length* tunnel as well. The main purpose though was to reduce the calculation time in future and more accurate models.
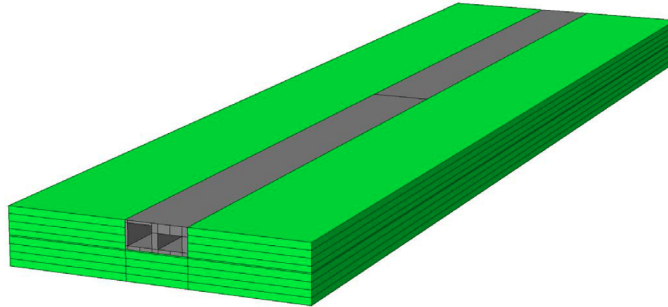
Figure 5.1: Linac's simplified model

The procedure carried out to prove the validity of the simplified model was to apply a harmonic point load in the middle of the walking path carrying out a frequency sweep and to compare the response of both the simplified (*half-length*) and the *full-length* model. The responses were compared at points located 7 m and 19 m towards both sides of the beam path's middle point and under the beam.
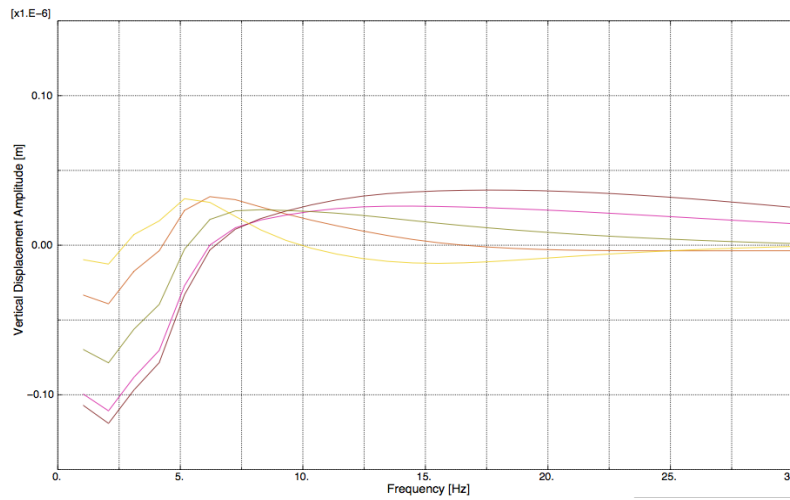
Figure 5.2: Displacement Amplitude [m] under the Linac's beam *full-length* model
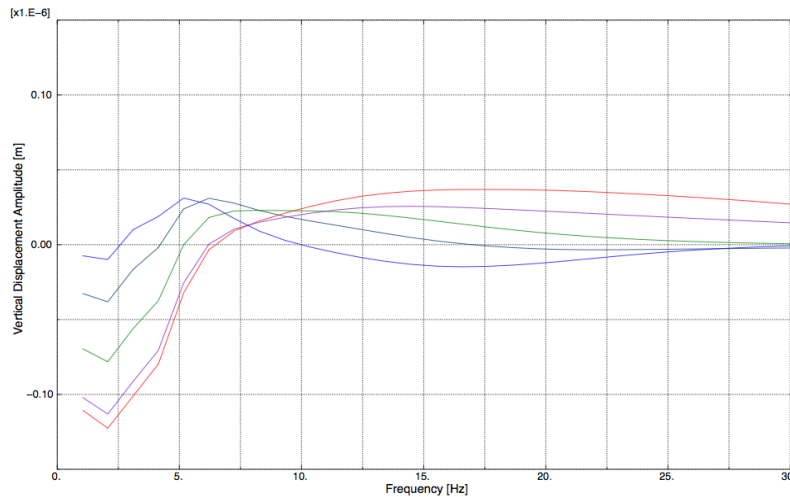
Figure 5.3: Displacement Amplitude [m] under the Linac's beam *half-length* model

As it can be seen in Figure 5.4, the responses are almost the same in both cases. Therefore, it can be concluded that a simplified *half-length* model could be used for the subsequent calculations. Hence, all the calculations in this study were carried out on the simplified *half-length* model.

5.5. Chosen Model

The model that finally was chosen and that produce the most accurate results is described in the following sections.

5.5.1. Linac

As it was previously introduced in section 1.3.1, the Linac was modelled as a unique section extruded along its way, not distinguishing between the different shapes of the cross-sections due to their negligible influence on the results.

The dimensions and shape of the Linac's cross-section are shown in Figure 5.4.
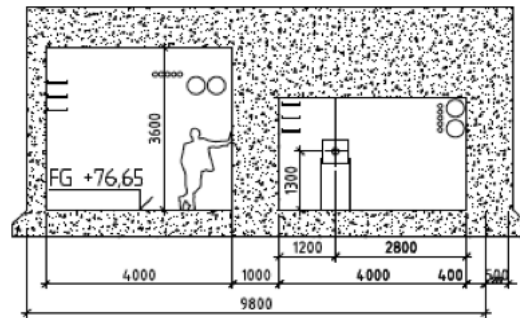
Figure 5.4: Linac's cross-section.

The total lengh of the Linac is 385 m, although in the simplified model it was extruded to a total length of 192.5 m. The Linac will be enterely built by concrete.

5.5.2. Soil

The modelling of the soil was discussed in section 5.3.2. It was created as a part around the Linac with a width of 50 m and a depth of 9.6 m, divided vertically in 8 different layers since its modulus of elasticity varies with the depth according to: $E(z) = 22 + 5z$ [MPa]. In the bottom further down, an infinite stiff layer was assumed (i.e. prescribed boundary conditions) due to the lack of properties regarding the bedrock. This is not totally true since a stiffer layer exists under the soil allowing reflections of the vibrations to be different. Thus, real results may differ a bit from the ones achieved in this study.

5.5.3. Bridge

A concrete bridge for bus traffic is planned to be built over the Linac, being the major external source of vibrations due to the road traffic. The bridge will be placed in such a way so it does not touch the Linac. The bridge will only be in contact with the soil and not the Linac.

Figure 5.5 shows a sketch of the bridge according to the drawings, [14].

(a)   (b)

(c)
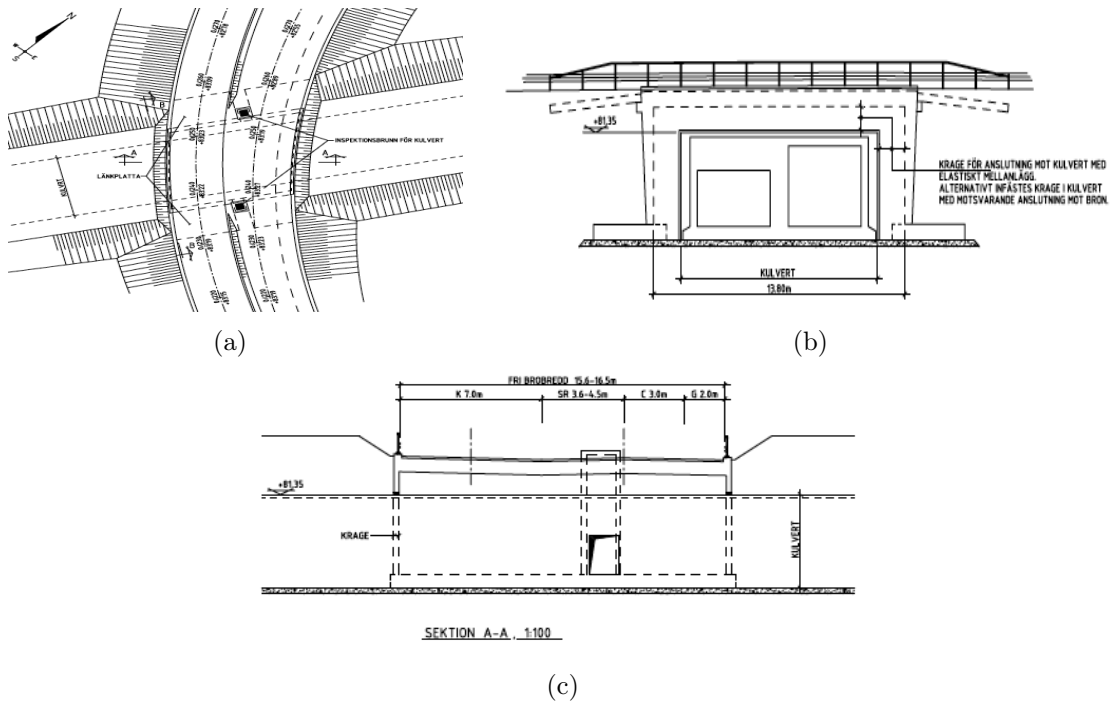
Figure 5.5: Bridge drawings

5.5.4. Road

A road with different layers was created as a continuation of the bridge at its both sides as shown in Figure 5.7. The model of the road was made from a typical section of a road as shown in Figure 5.6.
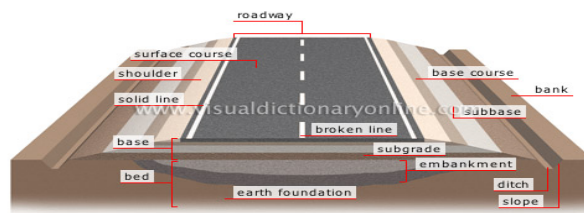
Figure 5.6: Typical road cross-section.

Table 5.3: Different layers of the road

Layer	z [m]	E[MPa]
Asphalt	0.17	400
Road base layer	0.2	350
Sub base layer	0.3	200
Bed / earth foundation	1.18	25

Each layer was consider to be stiffer than the previous one below, being the top surface layer (asphalt) ten times stiffer than the concrete as shown in Table 5.3. This value is not the real one of the asphalt, but it helps in the sense that the calculations are being performed for a conservative case. The damping was considered to be the same as for the concrete, i.e. $\zeta = 2\%$ for all the layers.
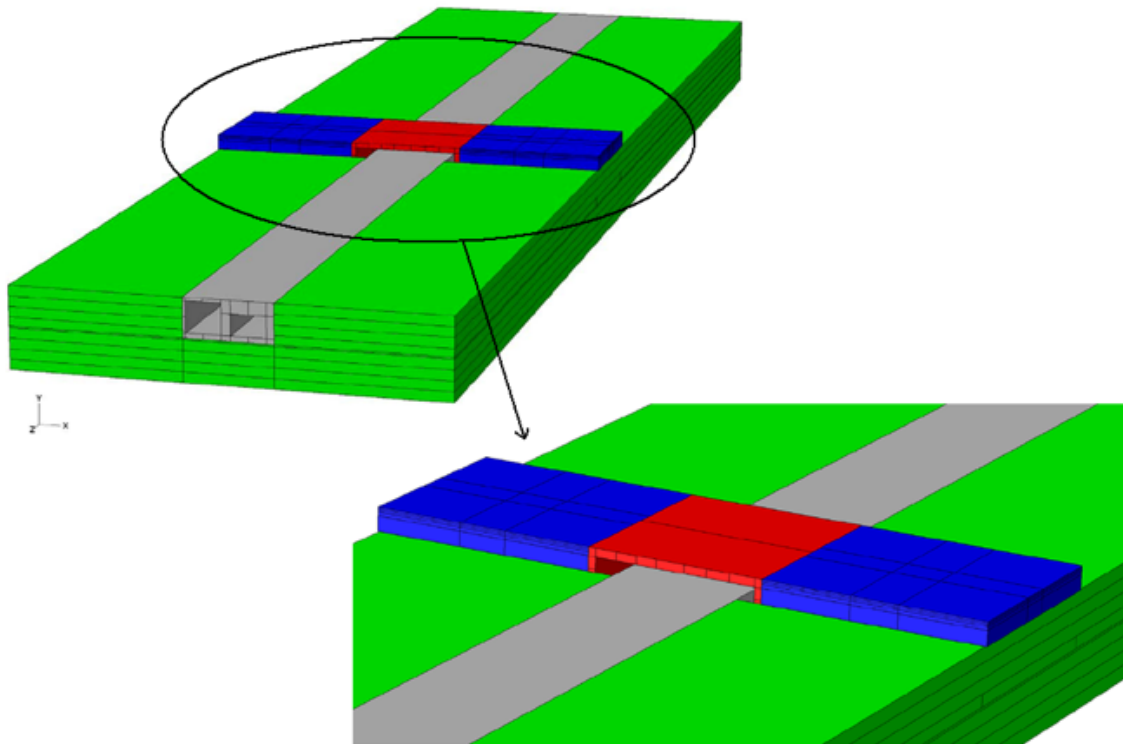
Figure 5.7: master thesis model.

Note that all the parts have fully interaction between them. This was modelled in *Abaqus* by a tie constraint at their common contact surfaces.

5.6. Mesh

All the parts in the model were meshed with solid isoparametric hexaedra linear elements, wich are the most common solid elements in three dimensions. Specifically, the elements used were C3D8I: 8-node linear bricks with incompatible mode. These first-order linear elements are essentially constant strain elements. They have three degrees of freedom on each node (no rotations, just translations in the three directions), [8].

In order to get reliable output from a dynamic analysis, it is advised that at least 6 nodes per wavelength should be considered, [8]. Since the elements used have linear interpolation, it can be concluded that 5 elements per wavelength are needed. For the soil and taking into account both shear and surface waves, an element should not be larger than 4 meters. Due to the fact that the wave speed is much greater in the concrete than in the soil, the concrete will not determine the upper limit of the element size. Of course the elements will not be set to a length of 4 meters, because this would lead to a very stiff structure, yielding not accurate results; but they will be in any case smaller.

On the other hand, the lower limit of the element size is determined by the computational cost (calculation time). The final size of the mesh is the result of a long and tedious process where a compromise between the computational cost and the accuracy in the solution was acquired. The size of the elements was reduced several times following a convergence process until one point where it was observed that the solution did not depend on the element size. Table 5.4 shows the summary of the number of elements, nodes and degrees of freedom on each part. It slightly varied from one case to another due to *Abaqus* features. This corresponds to the calculation with a road irregularity (section 6.4.2).

Table 5.4: Mesh details

Part	Nodes	Number of elements [C3D8I]	DOF
Bridge	13884	9950	41652
Soil	11500	9158	34500
Linac	106335	85422	319005
Road	2×2100	2×1500	2×6300
Total	135919	107530	407757

Therefore, It can be said that the upper limit of the element size in the mesh is determined by the wave length and the lower limit by the computational cost.

Figure 5.8: Meshed model

Linac's mesh	Bridge's mesh
Road's mesh	Soil's mesh
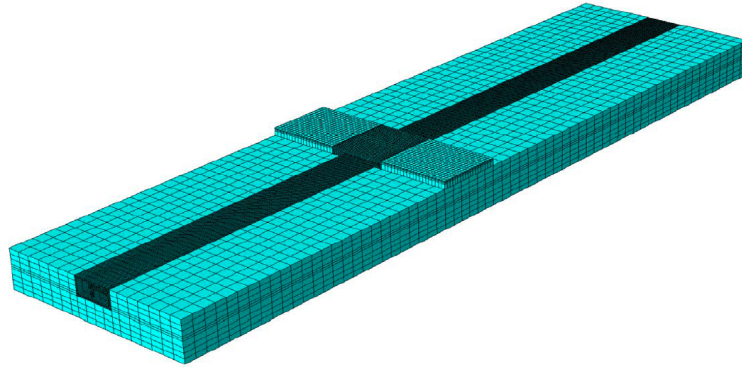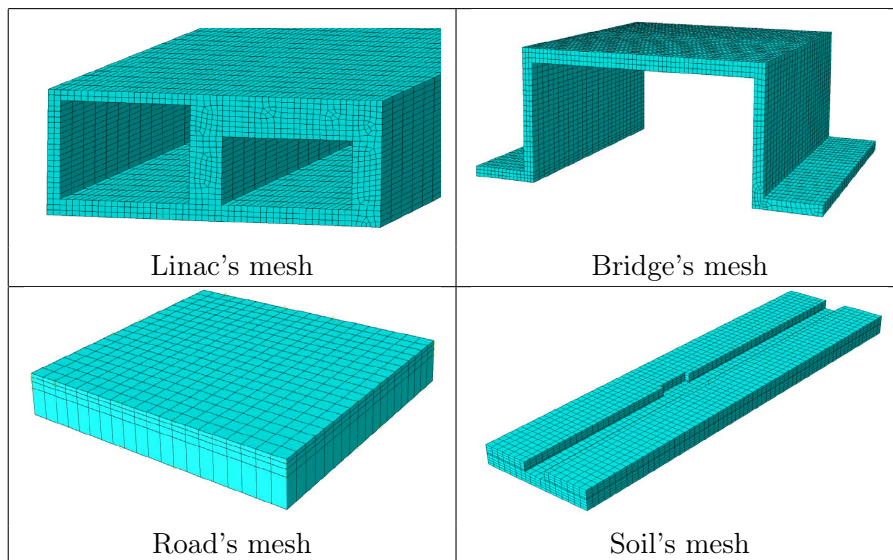
Figure 5.9: Detail of the mesh on each part

5.7. Damping

The are several options to introduce damping in a finite element model. As stated in section 2.5, Rayleigh damping was used in this study.

The main disadvantage of this kind of damping is that the material damping becomes dependent on the frequency as shown in the Eq.5.2.

$$\zeta_n = \frac{a_0}{2}\frac{1}{\omega_n} + \frac{a_1}{2}\omega_n \tag{5.2}$$

ω_n being the angular frequency at a natural mode.

The damping ratio is not constant for different modes of vibration.

When calculating the damping ratio of the concrete and the soil in the model, an approximation was made to determine a_0 and a_1 such that the damping was almost constant in the frequency range of interest which was set from 5 to 25 Hz. The reason of choosing this range was because the greatest displacement amplitudes in the previous try-outs done with a point load were obtained for this interval.

According to the literature [1], the damping ratio for the concrete has a value which may vary from 2% to 10%. However, there is a lack of knowledge regarding the properties of the soil. The damping ratio for soil is known to vary with the strain; i.e. it can vary from 1% for small strain to 20% with large strain. Due to this strain dependence, a different damping ratio should be considered for every load magnitude.

In the modelling, constant values for a_0 and a_1 inside the frequency range $(5-25$ Hz$)$ of interest for the damping ratio were chosen. An initial damping ratio of $\zeta = 20\%$ was considered but it was varied to check its influence on the response of the system.

To determine a damping that was as constant as possible within the frequency of interest, the Rayleigh damping parameters were determined from the critical damping. A "damping ratio versus frequency" plot was done for each material. Likewise, a tolerance for the varying damping ratio was set to $\pm 15\%$ of its initial value (both the tolerance and the frequency range are plotted as dashed lines as shown in Figures 5.11 and 5.10). Since the curve is inside the set tolerance within the frequency range, a_0 and a_1 can be assumed to be constant in the calculations. This values can be introduced in *Abaqus* as α and β respectively.

For the value considered in first instance, i.e. $\zeta = 20\%$, the values $a_0 = \alpha$ and $a_1 = \beta$ are calculated as follows (ω_i and ω_j are values inside the range):

For the concrete:

$$\alpha = a_0 = \zeta \frac{2\omega_i\omega_j}{\omega_i + \omega_j} = \frac{0.02 \cdot 2 \cdot 6 \cdot 19}{6 + 19} = 0.184 \tag{5.3}$$

$$\beta = a_1 = \zeta \frac{2}{\omega_i + \omega_j} = \frac{0.02 \cdot 2}{6 + 19} = 0.0016 \tag{5.4}$$

For the soil:

$$\alpha = a_0 = \zeta \frac{2\omega_i\omega_j}{\omega_i + \omega_j} = \frac{0.2 \cdot 2 \cdot 6 \cdot 20}{6 + 20} = 1.84 \tag{5.5}$$

$$\beta = a_1 = \zeta \frac{2}{\omega_i + \omega_j} = \frac{0.2 \cdot 2}{6 + 20} = 0.0154 \tag{5.6}$$
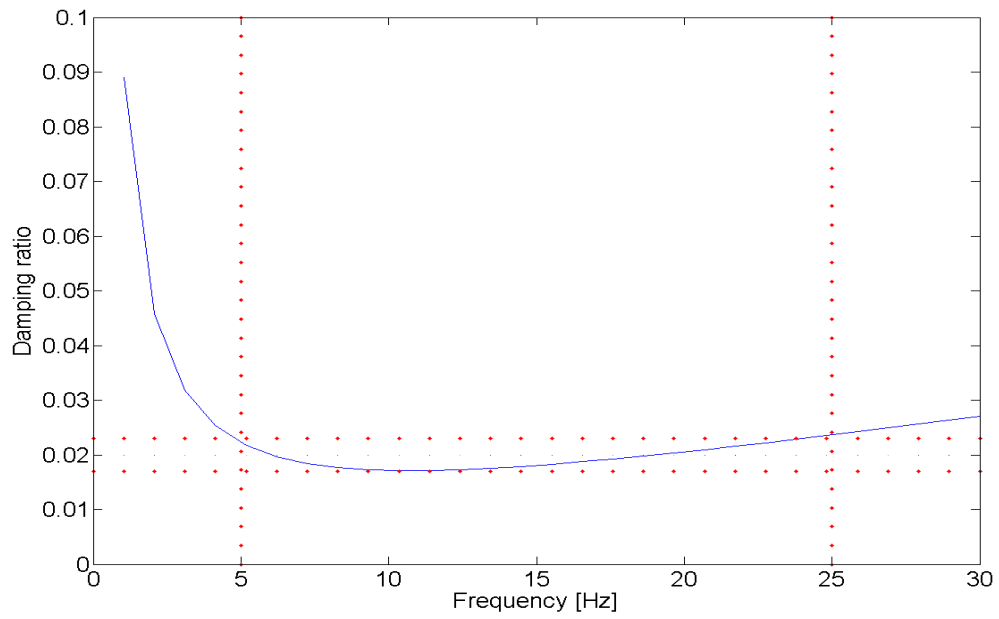
Figure 5.10: Damping ratio of the concrete vs frequency
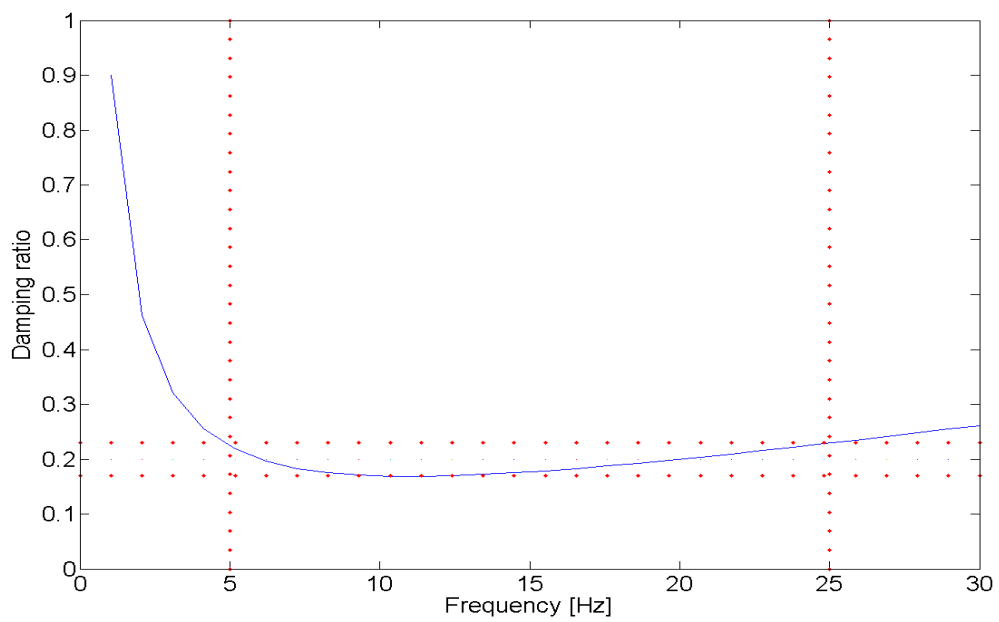
Figure 5.11: Damping ratio of the soil vs frequency

6. MODELLING RESULTS

6.1. Introduction

The vibration levels in the Linac tunnel were analysed by applying both harmonic and transient loads. For the harmonic loading, a parameter study was made by varying material properties. A simulation of the dynamic component of a bus load was also carried out. The use of discrete pillars was investigated too as a possible solution. For the transient loading, an irregularity on the road and a realistic walking load were simulated.

6.2. Evaluation Points

The technical requirement is meant to be fulfilled at the foundations where the magnets accelerating the beam will be mounted. The success of the researches performed inside will depend on the precision of the beam. Thus, all the displacement amplitudes shown in the graphs of this chapter were plotted on several points which are the so-called evaluation points, all of them located under the beam along the Linac.

As the foundations where the beam will be supported will have a high stiffness, it is assumed that the vibration levels on top of them will be the same as at their bottom. Hence, the evaluation points were chosen to be on the floor along the beam path.

6.3. Harmonic Load

In this section, a parameter study and an analysis simulating the dynamic component of a bus load will be investigated by means of harmonic loading. Likewise, the addition of discrete pillars was investigated as a possible solution.

6.3.1. Parameter Study

Several analyses were done in order to investigate the influence of several parameters in the model. A harmonic concentrated force f(t)=Asin(ωt) with an amplitude of 1 KN was applied in the middle point of the walking path. A frequency sweep

analysis was performed from 0 to 50 Hz in 1 Hz steps.

Note that all the points shown in figures 6.1, 6.2, 6.3 and 6.4 correspond to the maximum displacement amplitude for each case, no matter at which frequency they occurred. Note also that it is not the exact magnitude of the vertical displacement amplitude that is of interest in this section but the relation between the different choices of parameters. This load is very high and may not be realistic but since the response is linear the vibration levels obtained may be scaled to the load applied.

Density of the Soil

As previously mentioned, the density of the soil is an uncertain parameter due to the lack of data regarding the properties of the soil. Due to that, a variation of the density was carried out to investigate its influence on the response of the model.

Hence, the parameter was varied between two reasonable values, e.g. from $1400 \, \mathrm{kg/m^3}$ to $2200 \, \mathrm{kg/m^3}$ in steps of $100 \, \mathrm{kg/m^3}$. The result obtained by varying the density of the soil is shown in Figure 6.1. Due to the results shown, it can be concluded that this parameter has a minor influence on the response of the system since the displacement amplitude only varies by 2.4%.
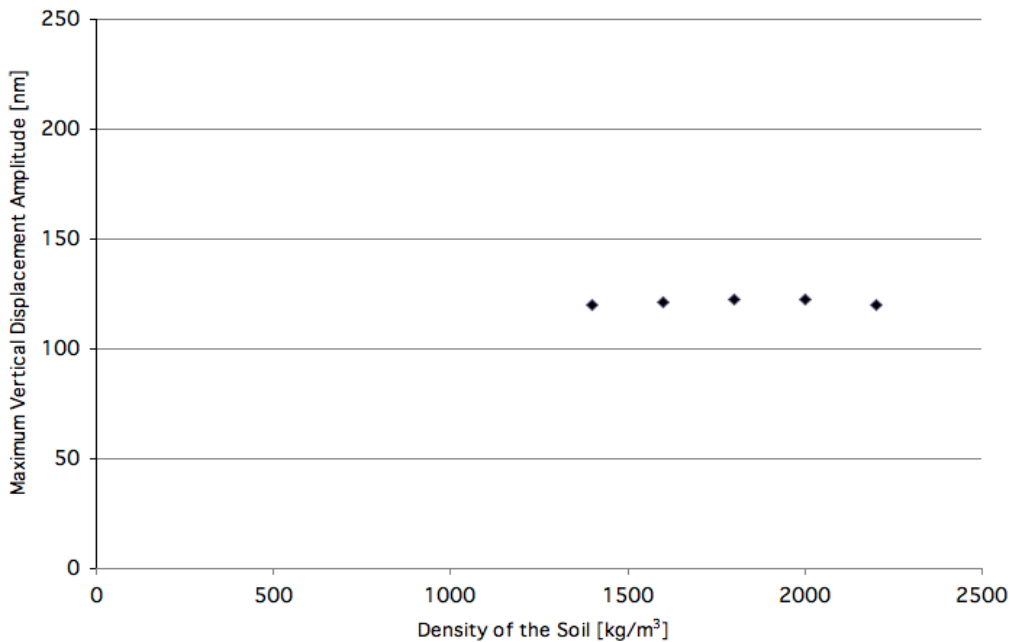
Figure 6.1: Vibration levels in the tunnel for different soil densities.

Modulus of Elasticity of the Concrete

Depending on the classification, the modulus of elasticity of the concrete may have different values and was thus varied from 35 GPa to 50 GPa in steps of 5 GPa.

As for the density, the modulus of elasticity of the concrete only shows a slight influence on the displacement amplitudes. Approximately 4.5% of variation was observed, as shown in Figure 6.2.
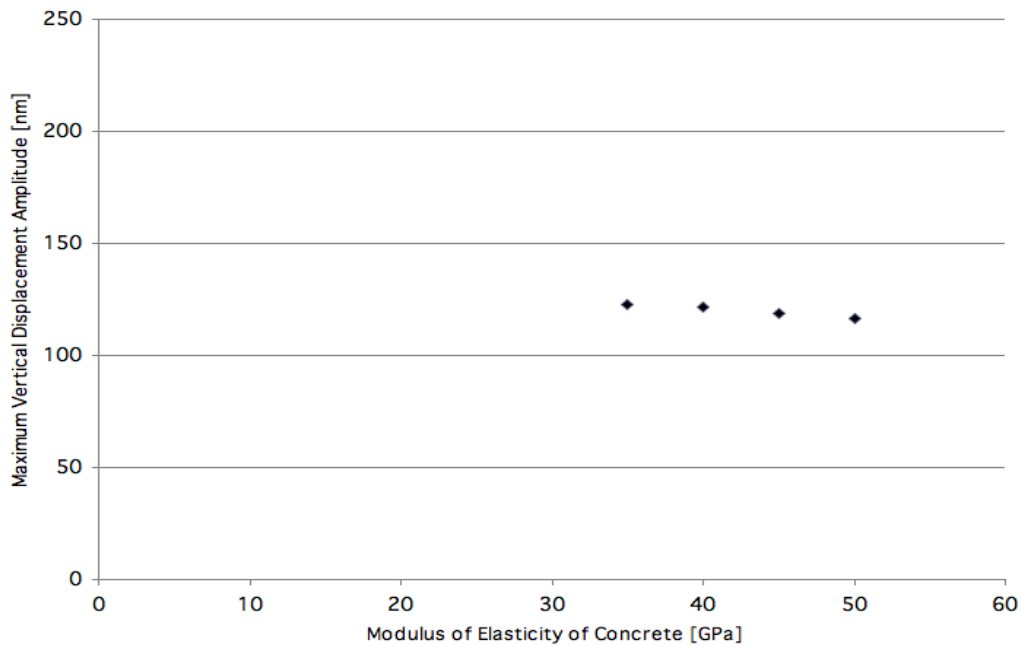
Figure 6.2: Vibration levels in the tunnel for different modulus of elasticity of the concrete.

Thickness of the Concrete Floor

The thickness of the concrete floor was also varied. All the activities and objects, e.g. walking, beam foundations, machinery, etc. are loading the floor of the tunnel. It is therefore an important parameter to take into account. Hence, the thickness of the floor of the whole tunnel was varied from 0.4 m to 1 m in steps of 0.2 m.

As shown in Figure 6.3, a benefit of increasing the thickness of the concrete floor is only effective up to 0.8 m. After this thickness, the maximum displacement amplitudes do not change to a great extent.
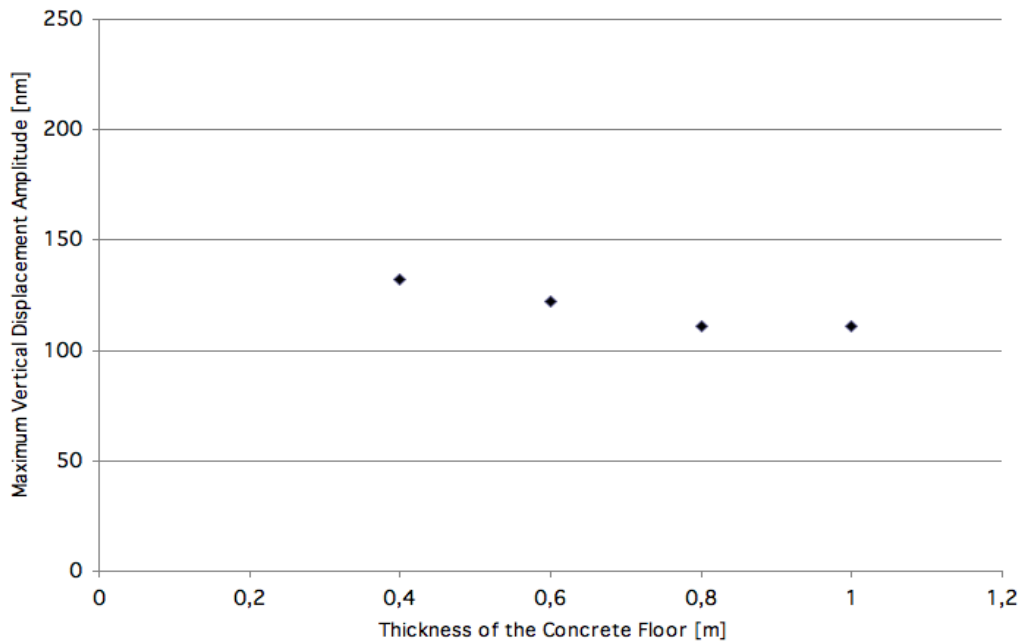
Figure 6.3: Vibration levels in the tunnel for different thicknesses of the concrete floor.

Damping Ratio of the Soil

The damping ratio of the soil was varied in the last instance. The importance of this investigation is evident since the damping ratio of the boulder clay is very uncertain and is strain dependent with a variation from 1% to 20%. Likewise, analyses with damping ratios of 1%, 2%, 5%, 10% and 20% were performed. The result is shown in Figure 6.4.

As opposed to the other parameters, soil damping does have a large influence on the vibration levels. A 96% variation of the response was obtained as shown in Figure 6.4.

It can be concluded that the displacement amplitudes under the beam depended a lot on the damping ratio of the soil. To fulfill the technical requirement, special attention regarding the properties of the soil should be paid. Moreover, some field measurement should be performed on site to determine its properties.
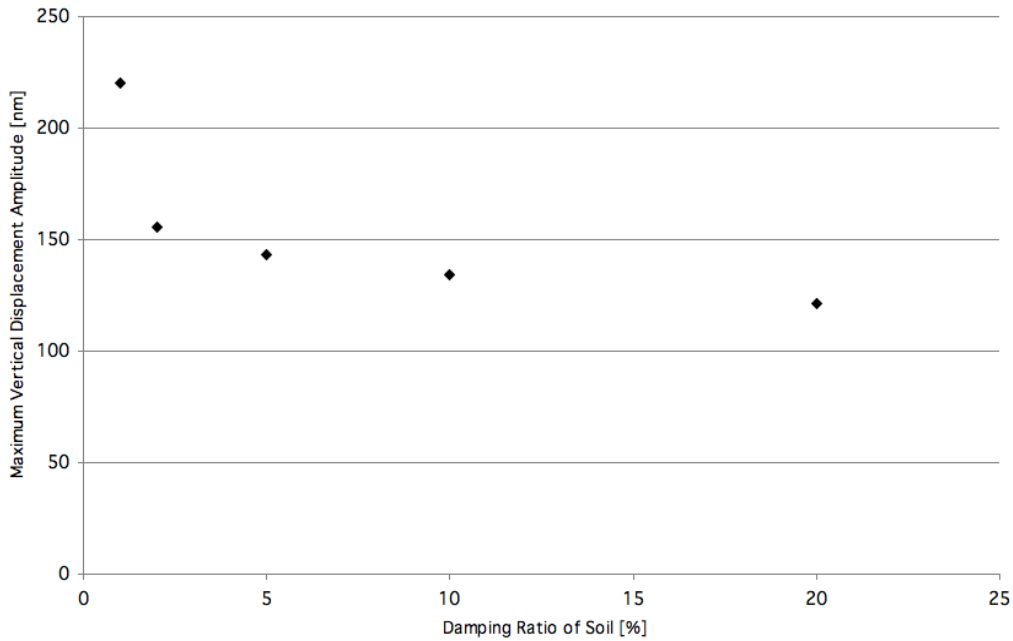
Figure 6.4: Vibration levels in the tunnel for different damping ratios of the soil.

6.3.2. Dynamic Component of a Bus Load on an Even Road

In contrast to discrete irregularities, random and periodic road surface roughness lead to continuous dynamic interaction forces between a traveling vehicle and the road. If the profile road surface includes a periodicity that at the posted speed leads to a forcing frequency, which coincides with any of the natural frequencies of the vehicle and/or those of the soil, substantial vibrations may be induced. Normally, this vibration generation mechanism does not play a major role in the case of road vehicles [6].

Due to the lack of traffic measurements in the future location of the Linac; it was necessary to study literature data [6]. Although the main aim of that study was to compare the vibration levels induced by two different types of buses (*Low-Floor System bus* and *Nova Classic bus*), it was considered that the newest one (*Low-Floor System bus*) could be assimilated to the same type of buses that will run on the bridge over the Linac. Hence, data from that paper was taken to determine the load magnitude on the bridge from a bus.

Given the need of modelling the bus load and due to the huge calculation time a moving mass crossing over the bridge would have, it was decided to substitute that moving mass by applying four concentrated harmonic forces instead (one per wheel) and then perform a frequency sweep from 0 to 50 Hz. Since only dynamic forces and not masses were applied, this analysis only takes into account the dynamic

component of the load. In Figure 6.5, a record of the typical time history of the
dynamic load component induced by the test bus passing over a wood plank is shown.
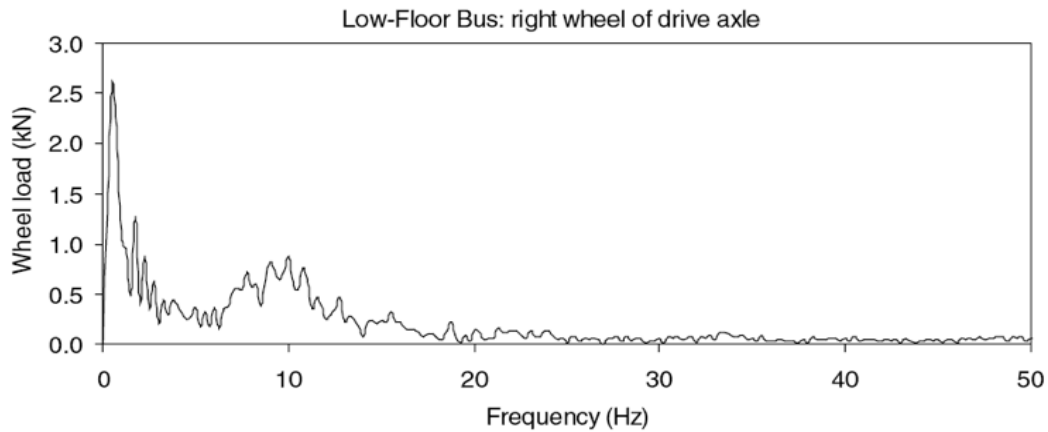
Figure 6.5: Narrow band frequency spectra of dynamic load induced by test buses passing
over a wood plank on road surface at 50 km/h.

The data in Figure 6.5 corresponds to a bus passing over a plank, but here the load
from a bus on smooth asphalt is to be analysed. An average wheel load value should
be considered in order to simulate the behavior of the bus over an even surface. A
value of 0.6 kN per wheel was assumed by studying the latter part in Figure 6.5.
According to [6], the study was accomplished with "no passengers or dead weight",
so an increment of this wheel load should be taken into account in order to sum up
the dynamic component of the load that passengers could induce. Thus, a load of
4×0.7 kN was considered.

Three analyses were made where the location of the bus load was varied trying to
find the worst scenario.

Bus on the Road

In the first load case, the four loads representing the wheels were placed in the mid-
dle of the road as shown in Figure 6.6. The maximum displacement amplitude in
the beam tunnel was for this case found to be 92.6 nm as shown in Figure 6.7.
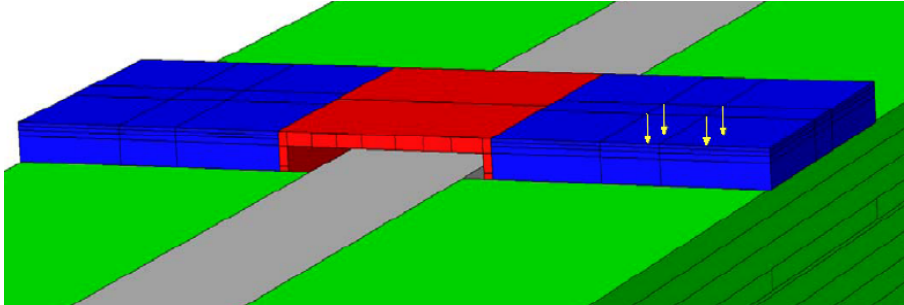
Figure 6.6: Bus on the road
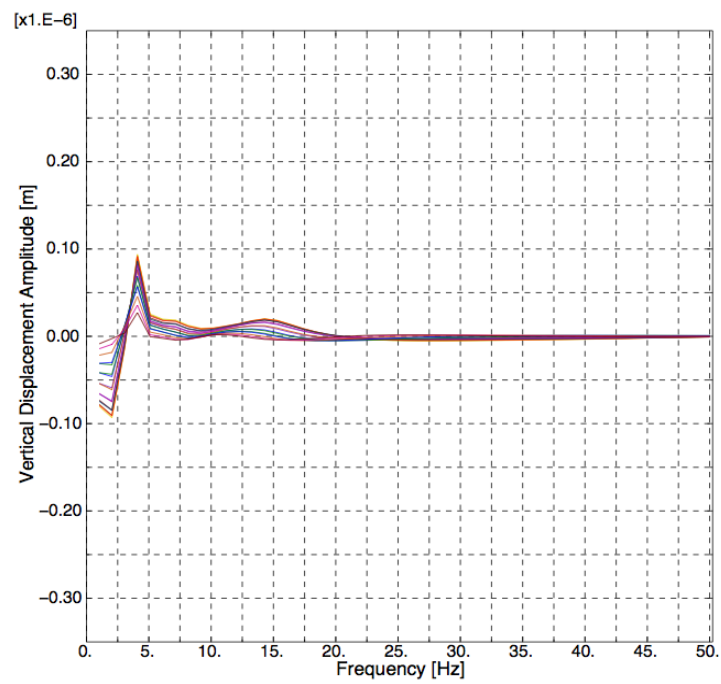
Figure 6.7: Displacement amplitudes on the beam tunnel floor.

Bus on the Bridge

In this case, the four loads representing the wheels of the bus were placed right in the middle of the bridge as shown in figure 6.8. The obtained displacement amplitudes of the structure are shown in Figure 6.9. The maximum displacement in the beam tunnel was found to be 197.1 nm.
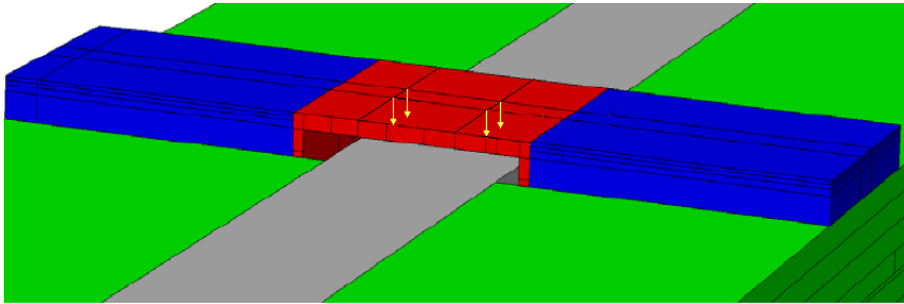
Figure 6.8: Bus on the bridge.
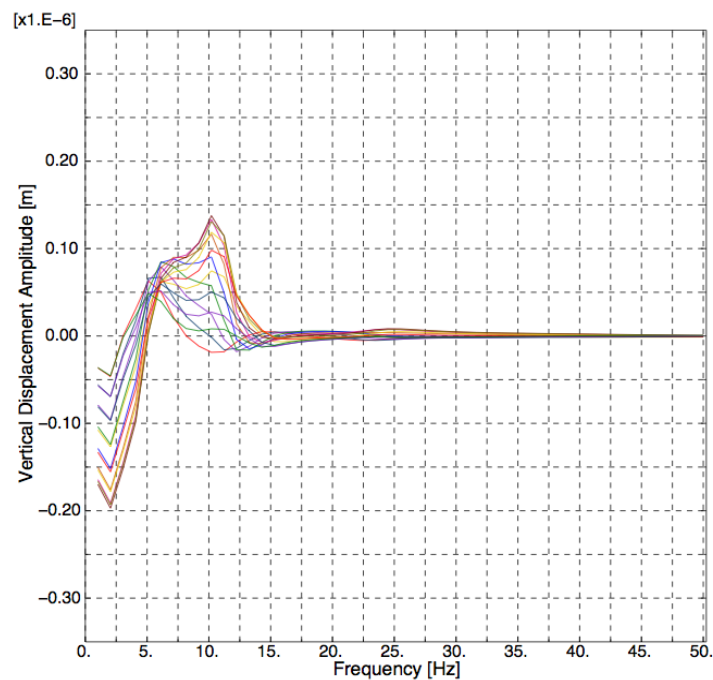
Figure 6.9: Displacement amplitudes on the beam tunnel floor.

Bus in Between the Bridge and the Road

In this case the bus was considered to be simultaneously on the bridge and on the road. Thus, two forces were placed on the bridge and two forces were placed on the road as shown in Figure 6.10. The maximum displacement amplitude was for this case 301.6 nm which was found to be the worst case in terms of the location of these 4 harmonic forces, as shown in Figure 6.11.
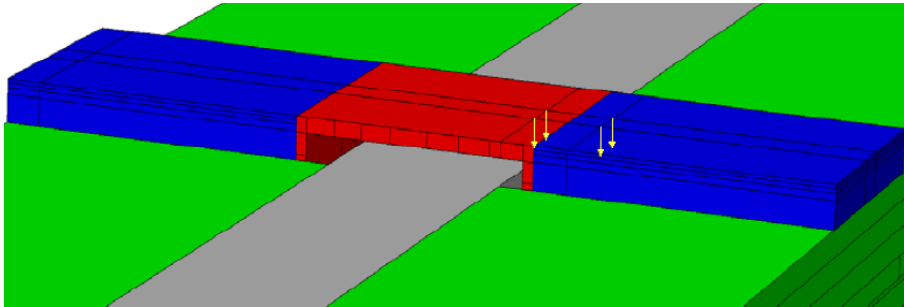
Figure 6.10: Bus in between the bridge and the road.
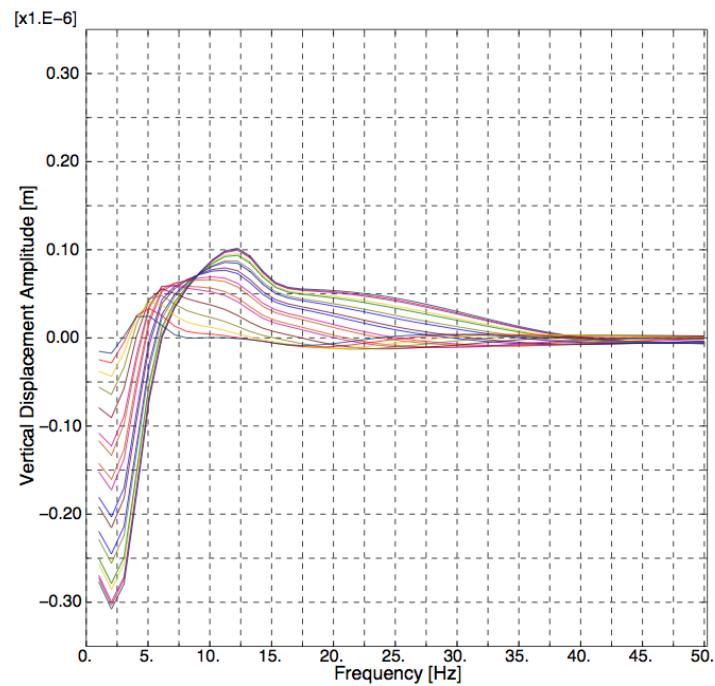
Figure 6.11: Displacement amplitudes on the beam tunnel floor.

6.4. Transient Loads

6.4.1. Introduction

Traffic and walking loads were simulated to determine vibration levels for two re-
alistic load cases. Being transient loads, they have an arbitrary time variation and
duration with any periocity, see Figure 6.12.
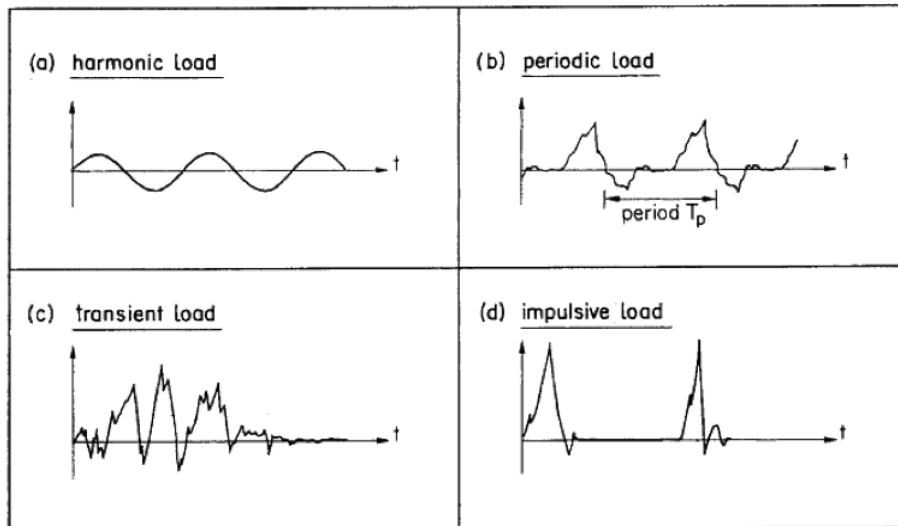
Figure 6.12: Different types of loads.

6.4.2. Road Irregularity: Pulse Load

It is well-know that the most severe traffic vibrations are created by heavy vehicles
moving rapidly along roads. And even more if it has some type of irregularity [6].
A good and obvious way to reduce vibrations would be by keeping trucks and buses
away from the facility. Since this is impossible in this case because a bridge over the
Linac is planned to be built; "speed bumps", potholes, bumps, expansion joints...
should not be permitted close by. Anyway and in order to cover and take into con-
sideration all the cases (specially the worst ones); a calculation with an irregularity
on the road was performed. Furthermore, velocity restrictions could also be applied
in the surroundings of the facility, since this parameter has a large influence in the
vibration level created [6].

The frequencies created by vehicles moving along roads depend on many different
factors such as: conditions of the road, vehicle weight, speed, type of the suspensions
system; soil type and stratification; season of the year; distance from the road and
building type [6].

The data for the pulse load was also determined from [6].

Creating the Bus Load

The load resulting from a bus or a truck hitting a road surface irregularity is composed of an initial impact force and an oscillating force from the subsequent "axle hop" of the vehicle, [6]. The impact generates ground vibrations that are predominant at the natural frequencies of the soil whereas the axle hop generates vibrations at the hop frequency (a characteristic of the vehicle's suspension system). Of course, if the natural frequencies of the soil coincide with any of the analysed structure, resonance occurs and vibrations will be amplified, [6].

The "pulse load" was modeled only taking into account this first initial impact of the recorded wheel-load versus time diagram shown in Figure 6.13.
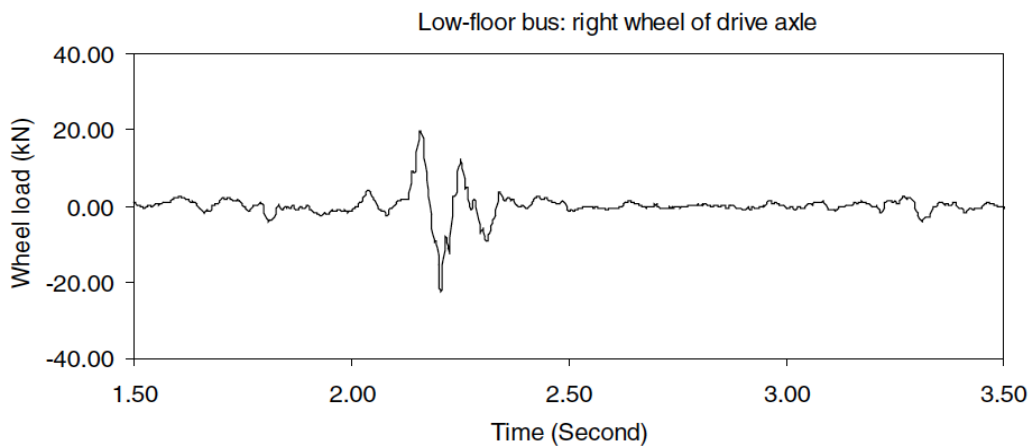
Figure 6.13: Typical time records of dynamic load components induced by test buses passing over wood plank on road surface at 50 km/h.

In [6], bus traffic vibrations were measured when its right wheel passed over a wood plank with the dimensions 3.7 cm high, 13.8 cm wide and 90 cm long. As shown in Figure 6.13, the bump coincides with the first peak around 2.15 seconds. Since the simulation here only was assumed to consider the wheels passing a single imagined displacement on the road, only the first pulse in Figure 6.13 was considered. The pulse load was created as follows:

1. Time and force measurements of the first impact were taken from Figure 6.13.

2. A time record of the initial bump impact was extracted and scaled from 6.13 in order to simulate it in *Abaqus*.
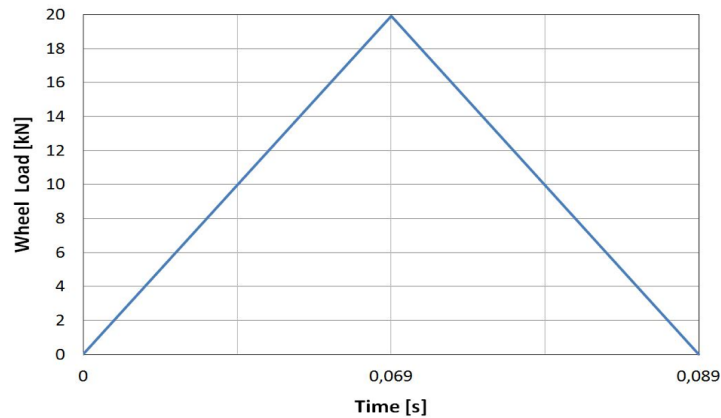
Figure 6.14: Time record of the pulse load.

In order to simulate the irregularity on the road, three transient forces located in three different places and separated from each other a reasonable distance (see Figure 6.15) were applied with a magnitude of 19.90 kN. The reason of placing three pulse loads was just to find the worst scenario. The time history is shown in figure 6.14. A transient analysis was performed during three seconds. The resulting displacement amplitudes obtained from the analysis is shown in Figure 6.16.
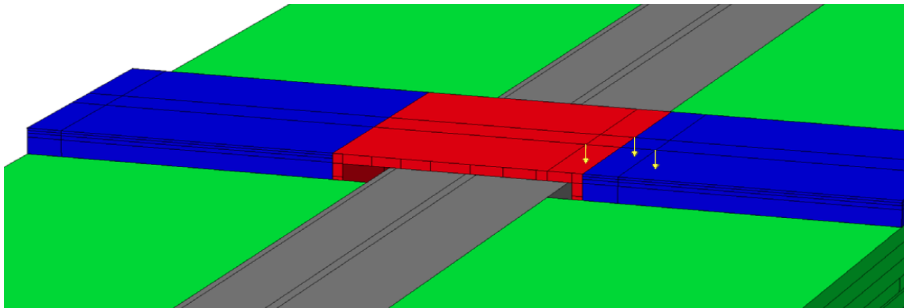
Figure 6.15: Location of the bumps.

Note that the worst situation is when the bump is placed on the bridge and close to where the road and the bridge are joined together as shown in the third negative peak in Figure 6.16.

In order to check the fulfillment of the technical requirement, a code was created using *Matlab*. Data was extracted from *Abaqus* from which the second with the highest RMS displacement was determined.
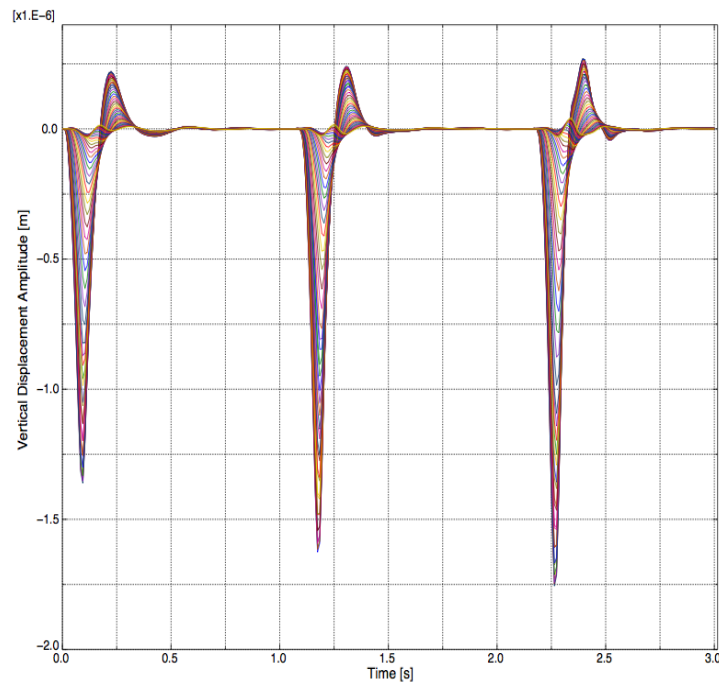
Figure 6.16: Displacement amplitudes om the beam tunnel floor.

The obtained resulting RMS value was $u_{RMSmax} = 365.1$ nm wich is obviously much greater than the permitted value of 100 nm.

6.4.3. Walking Load

Man Induced Vibrations

Human walking may be regarded as a dynamic load. Walking is a periodical movement on a flat surface in which two feet move alternately from one position to another and do not leave the surface simultaneously. Walking loads can be completely defined by seven parameters, [16].

1. Static characteristics

    1. Load intensity

    2. Location

2. Dynamic characteristics

    1. Load amplitude

    2. Frequency range

    3. Phase lag

4. Crowd effect

5. Moving velocity

The load amplitude, phase lag, frequency and crowd effect are the keys for defining the loads as it will be seen afterwards.

The model of individual walking loads, similar to jumping loads, can normally be expressed by Fourier series if they are assumed to be a periodic activity.

$$F(x,t) = G(x) + [1.0 + \sum_{n=1}^{n} r_n sin(2\pi n f_p t + \phi_n) \tag{6.1}$$

where

G is the load intensity (weight of the person)
r_n is the load factor (Fourier coefficient)
x is the load position
ϕ_n is the phase lag
f_p is the load frequency (activity rate).

Human Walking

Walking is a periodic excitation. According to [10], the step frequencies ussually oscillate between 1.5 and 2.5 Hz (depending naturally on the activity). Therefore, walking could of course cause resonance when exciting some of the natural frequencies or the fundamental frequency of a structure.

Figure 6.17 shows the reaction force time history for one step divided into separate time histories for the heel and the forefoot respectivelly, [7].
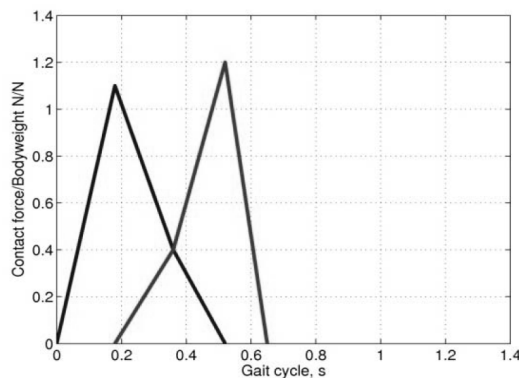
Figure 6.17: Reaction force time history for one step divided into separate time histories for the heel and the forefoot.

Since the Linac model is much greater compared with a foot length, it was considered that the distinction between the heel and the forefoot could be perfectly avoided so just a distinction between both feet was taken into account as shown in Figure 6.18.
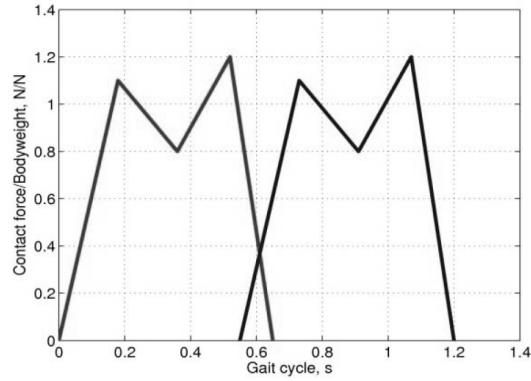
Figure 6.18: Reaction force of a gait cycle for two steps.

FE Simulation

The human walking was modelled as a moving load in *Abaqus*. Several points distributed following a gait cycle pattern were created on the walking path of the Linac, see Figure 6.19. Concentrated point loads were placed on positions simulating a foot, as shown in Figure 6.20. A time history was created for each foot load simulating the pedestrian walking. The time period of a gait cycle is 0.55 s which results in a gait frequency of 1.8 Hz, [7].

Parameter	Value [cm]
l_1	26.5
L_1	65
L_2	65
d_1	5
d_2	5
d_3	2.2
D_1	10
D_2	19
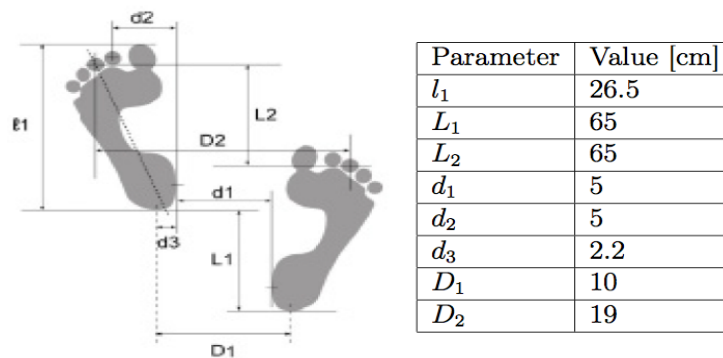
Figure 6.19: Different parameters used for the calculation.
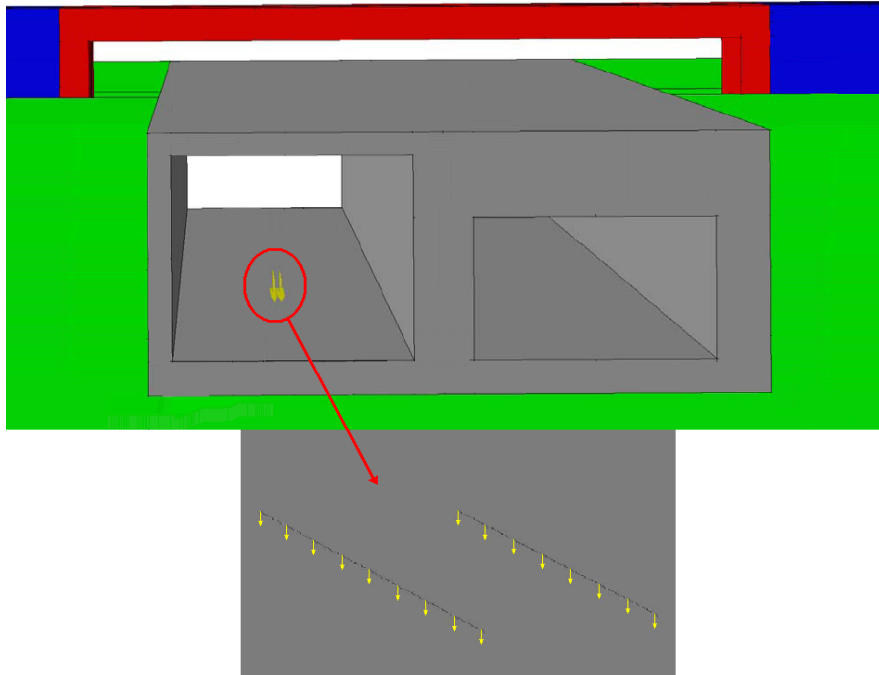
Figure 6.20: Detail of the gait cycle

Note that the y-axis in Figure 6.18 has the units of force/weight. This is because, according to [10], the weight of a person does not significantly affect the shape of the pattern, just the magnitude of the force. A 75 kg person was considered in the calculations. Full transient analysis were carried out during 5 s with a time-step of 0.01 s.

The Linac's requirement states that a RMS value of 100 nm in the vertical direction of the displacement should be never exceeded during one second. The same *Matlab* code as used in section 6.4.2 was used to determine the highest RMS value during 1 s. The RMS value for the second with the highest value was 56.01 nm, which is less than the 100 nm that the requirement for the Linac. Note that in this simulation only the gait cycle of one person was considered, so this value could dangerously increase when groups of people walk together through the walking path and therefore close to the beam line.

Moreover, in Figure 6.21 the displacement amplitudes under the beam are shown to follow the shape of the load amplitude of the gait cycle but a little bit delayed.

Note that in the calculation both the static and the dynamic part of the load were considered. In the requirements, the static part is not accounted for when calculating the RMS value.
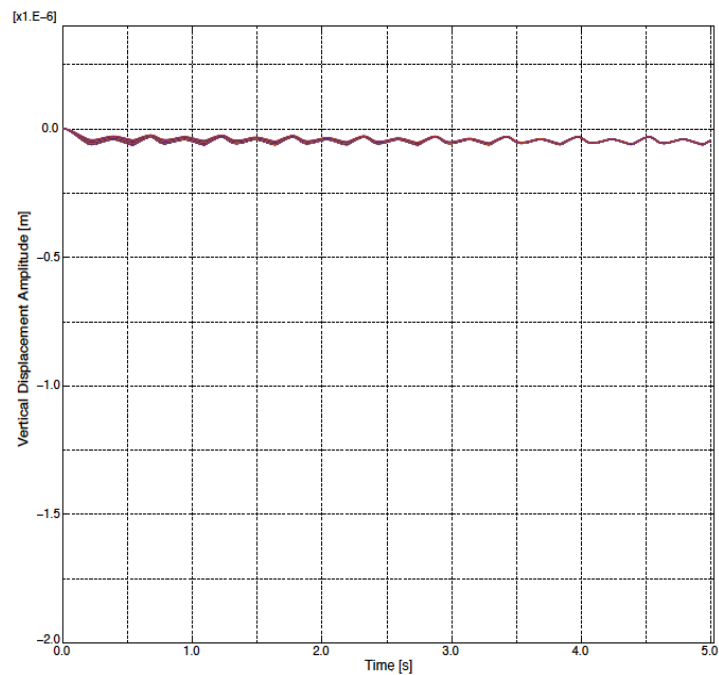
Figure 6.21: Displacement amplitude under the beam due to the walking load

6.5. Pillars

An obvious need of pointing out some solution could be noticed after seeing the results obtained in the previous calculations, since in some of them the technical requirement was not fulfilled.

One solution tried was the addition of pillars under the bridge. Thus, columns (diameter of 40 cm) were driven down from the bridge as shown in Figure 6.22.

(a) One pillar (b) Two pillars
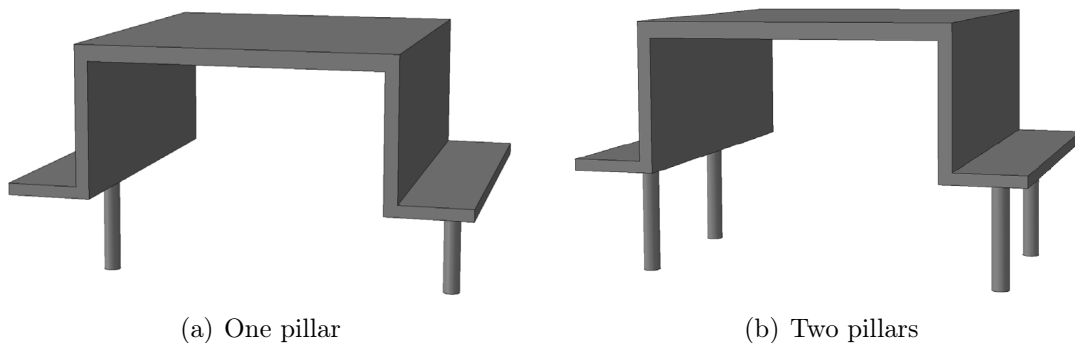
Figure 6.22: Addition of pillars underneath the bridge

Note that in this investigation the bedrock was considered. In all the previous cal-
culations it was avoided setting prescribed boundary conditions in the bottom of the
soil, but this was not totally true since a stiffer layer exists under the soil allowing
reflections of the vibrations to be different. Hence, a 10 m thick layer as stiff as con-
crete was created underneath the soil. Even though the properties of the bedrock
may not be exactly the same as concrete's, it was considered that this would lead
to more reliable results.

Moreover, the displacement amplitude was evaluated for the different cases, i.e. with
no pillars, one and two pillars respectively. The load applied was such as the one
considered in section 6.3.2, with two 1 kN harmonic loads placed on the bridge and
two on the road. The displacement amplitudes for the different cases resulting from
the different frequency sweeps are shown in Figure 6.23.

Figure 6.23 shows that the construction of pillars does reduce the maximum vertical
displacement amplitude under the beam, but not as much as it could be expected
beforehand. The very few pillars modelled do not stiff the structure enough and
their distribution is not the best one for the modal shapes which cause the highest
displacement amplitudes. Nonetheless, this investigation marks a trend to follow in
order to find a better disposition and number of pillars which effectivelly reduces
the vibration levels under the beam.

Figure 6.23: Influence of pillars

7. DISCUSSION

As proved on the Parameter Study, the properties regarding the soil have a great influence in the vibration levels of the floor, especially the damping ratio. The lack of data regarding the properties of the soil makes the analysis result uncertain. As it is the key issue in the model; a little variation on its properties could lead to completely different results. Therefore, it is of vital importance their determination through on site measurements in order to get reliable output which can be constrasted with the requirement. The parameter study, however, shows the influence of the various parameters irrespective of the absolute value.

Regarding a bus passing the bridge on a road that is constituted of smooth asphalt, it was proved that the requirement may be reached in that case. However, small irregularities on the road at the bridge will result in pulse loads that always will occur if the road is not in perfect condition or if, for example, ice, snow, potholes and objects like branches, soil and small rocks exist on the road. They will create vibration levels that are too high and the quality of the measurements at the MAX IV will be affected. Since the probability of not always having a smooth road is rather high, especially during the winter, it is recommended that the bridge is avoided and that the road will be relocated to not crossing the Linac.

Moreover, walking loads should also be taken into consideration since it was proved that they can cause high RMS values. Thus, groups of people could cause the requirement to be exceeded.

The addition of pillars was proved to be effective, but not to a great extend. Another distributions and number of pillars should be investigated.

8. Suggestions for Further Work

As previously stated, the properties of the soil should be determine through on site measurements in order to get a reliable output that can be compared with the requirements.

Besides, some realistic loads as impacts, machinery, groups of people walking together, etc. should be simulated in order to have a more realistic knowledge of the structure. In that results, a FFT should be done to take the leap between the time domain and the spectrum in order to see the its frequency content. Low components may be excluded from the RMS calculation.

Likewise, traffic simulations from the freeway E22 nearby the Linac should be taken into account as it can be an important external source of vibrations for the Linac. Furthermore, in this simulation the ring could be added making a combined model. The tunnel could act as a vibration barrier for the ring, reducing the vibration levels in the main facility for the benefit of the researches performed inside.

New distributions of pillars should be investigated in order to find a lay-out which reduce more effectivelly the vibration levels under the beam.

Likewise, variations in the geometry of the bridge could also be tried in order to check its influence on the response of the structure.

A. Appendix

A.1. Figures Steady-State Analyses
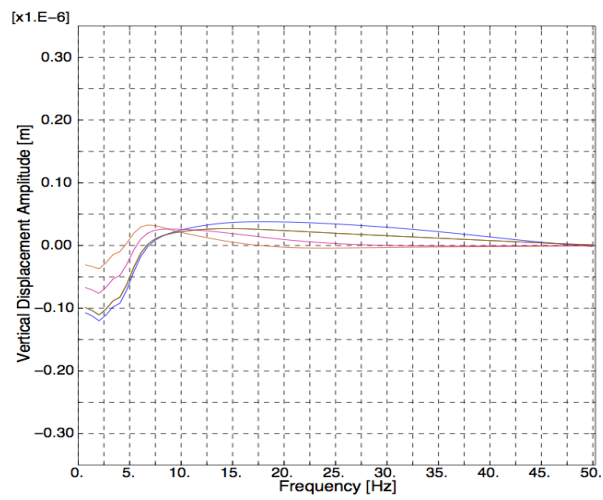
Figure A.1: Displacement vs frequency, density of soil is 1400 kg/m^3
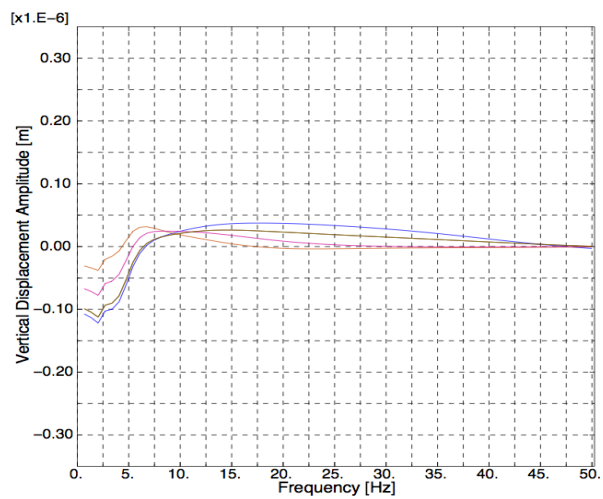
Figure A.2: Displacement vs frequency, density of soil is 1600 kg/m^3
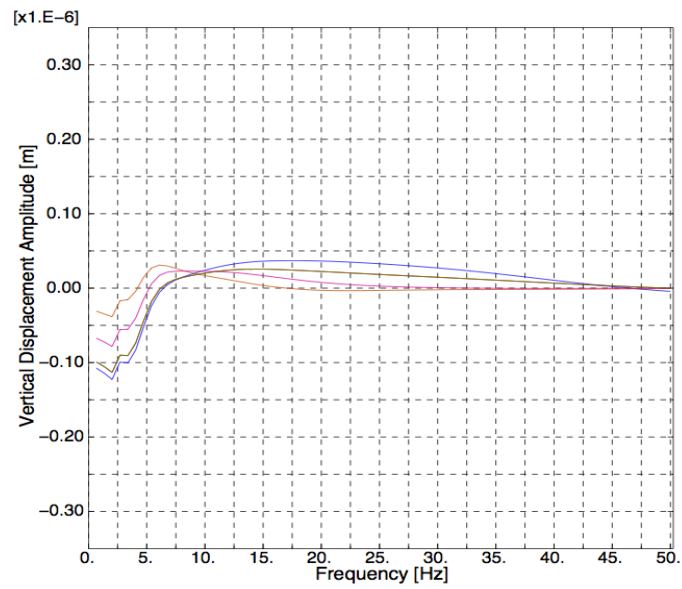
Figure A.3: Displacement vs frequency, density of soil is 1800 kg/m^3
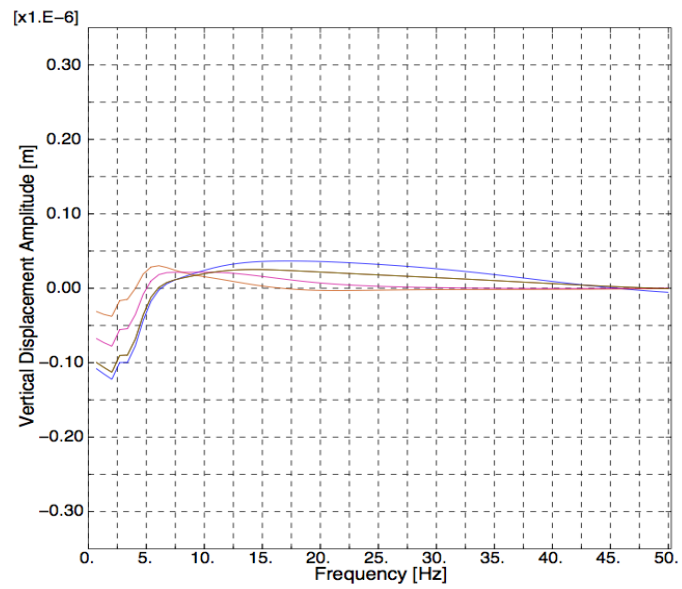
Figure A.4: Displacement vs frequency, density of soil is 2000 kg/m^3
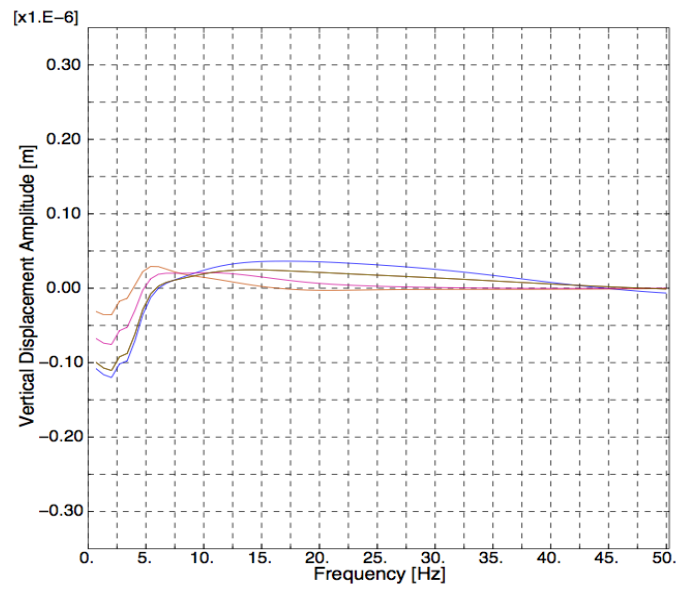
Figure A.5: Displacement vs frequency, density of soil is 2200 kg/m^3
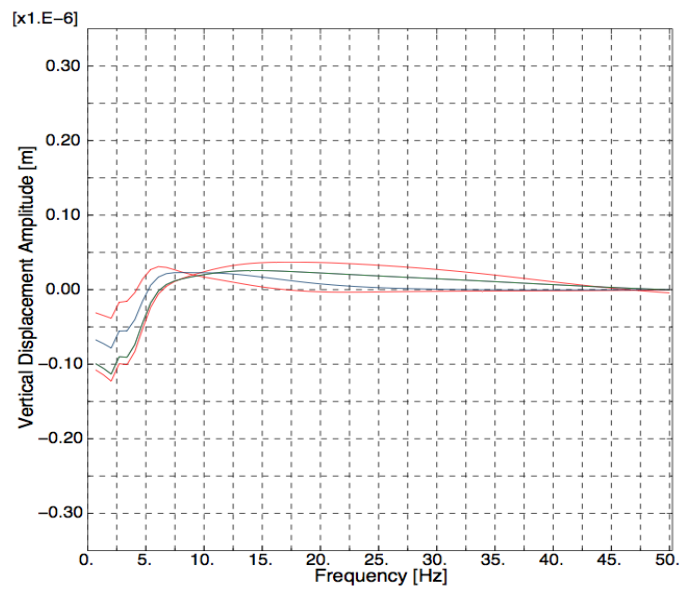
Figure A.6: Displacement vs frequency, Young's modulus of concrete is 35 GPa
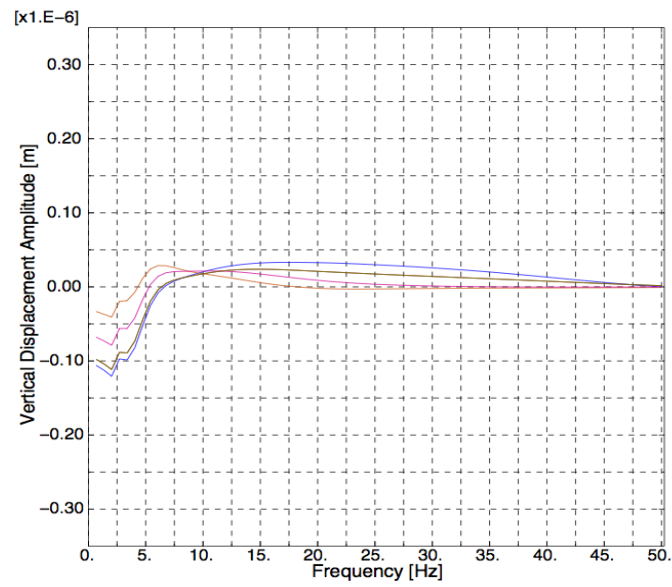
Figure A.7: Displacement vs frequency, Young's modulus of concrete is 40 GPa
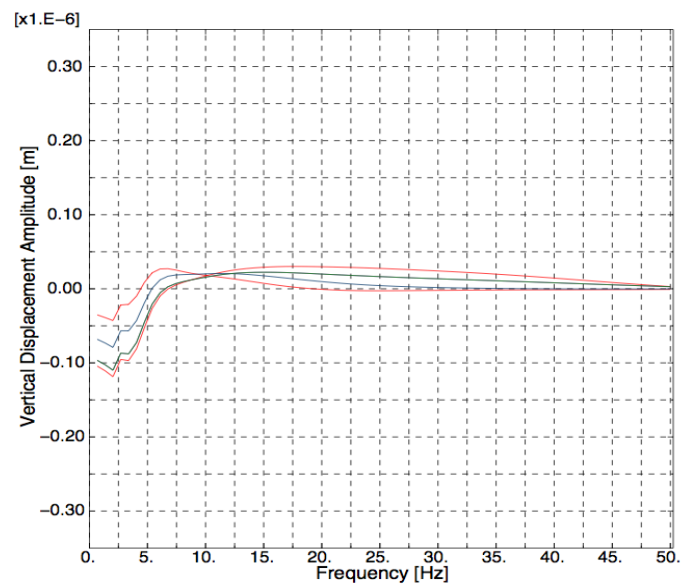
Figure A.8: Displacement vs frequency, Young's modulus of concrete is 45 GPa
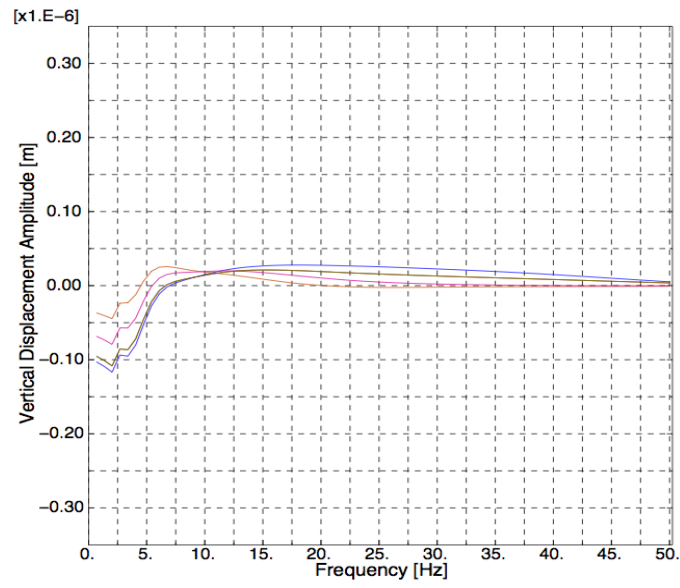
Figure A.9: Displacement vs frequency, Young's modulus of concrete is 50 GPa
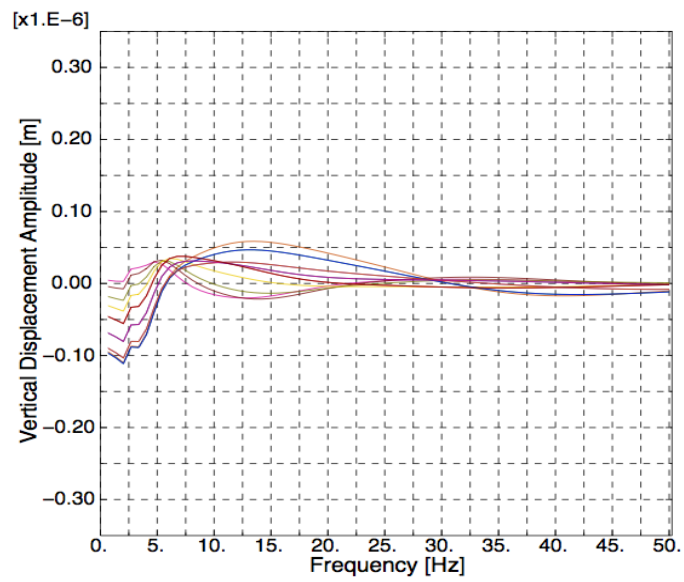
Figure A.10: Displacement vs frequency, floor thickness of 0.4 m
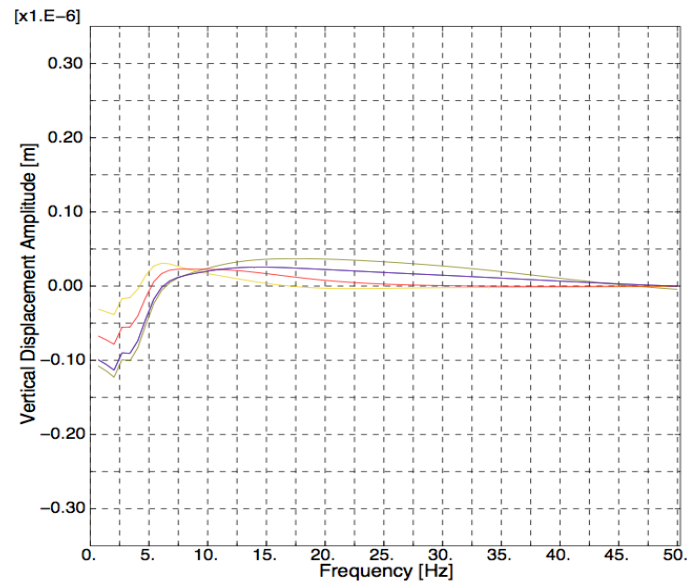
Figure A.11: Displacement vs frequency, floor thickness of 0.6 m
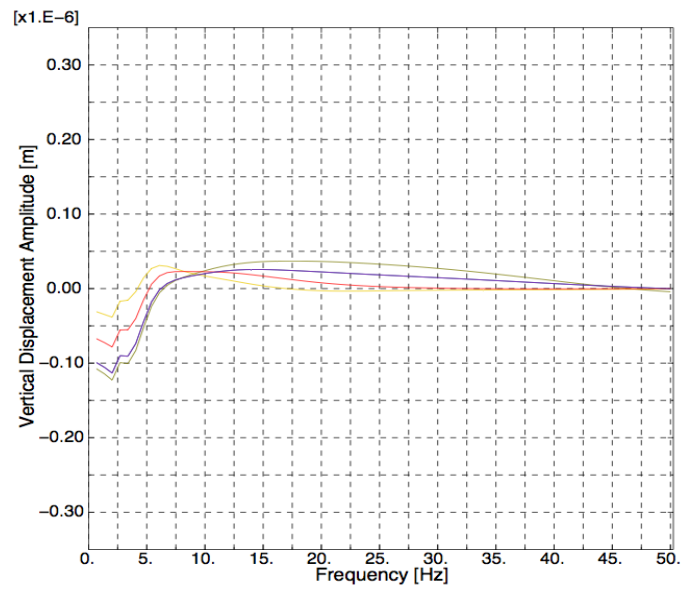
Figure A.12: Displacement vs frequency, floor thickness of 0.8 m
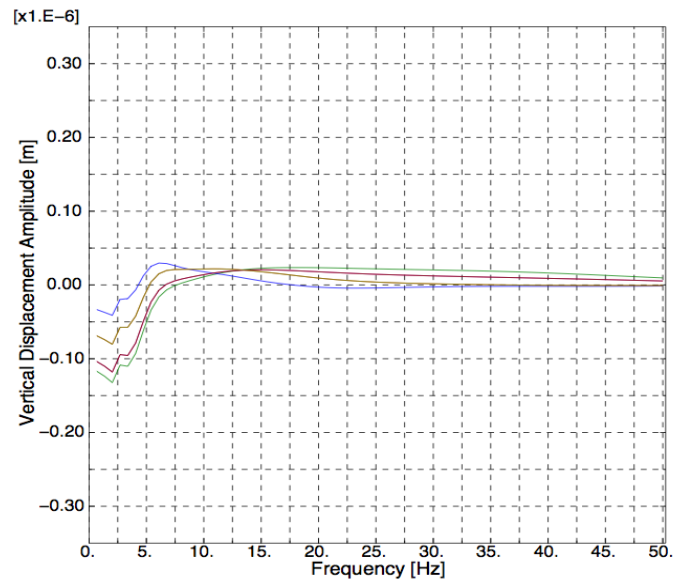
Figure A.13: Displacement vs frequency, floor thickness of 1 m
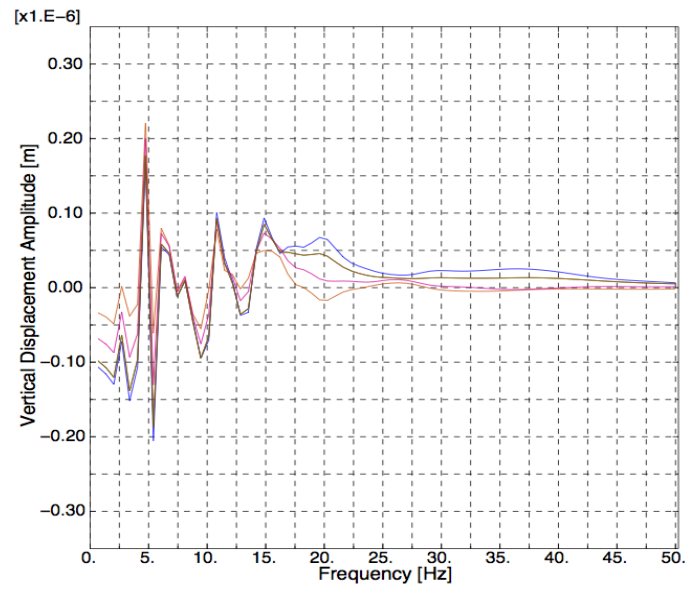
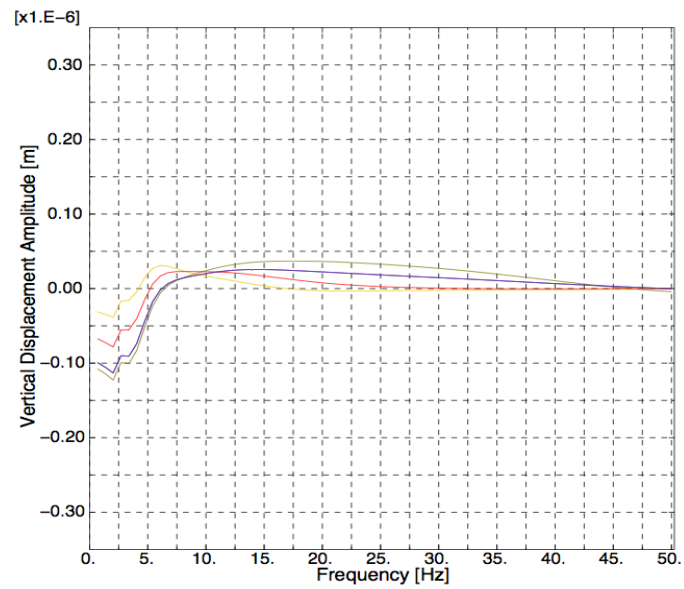Figure A.14: Displacement vs frequency, damping ratio of the soil is 1%
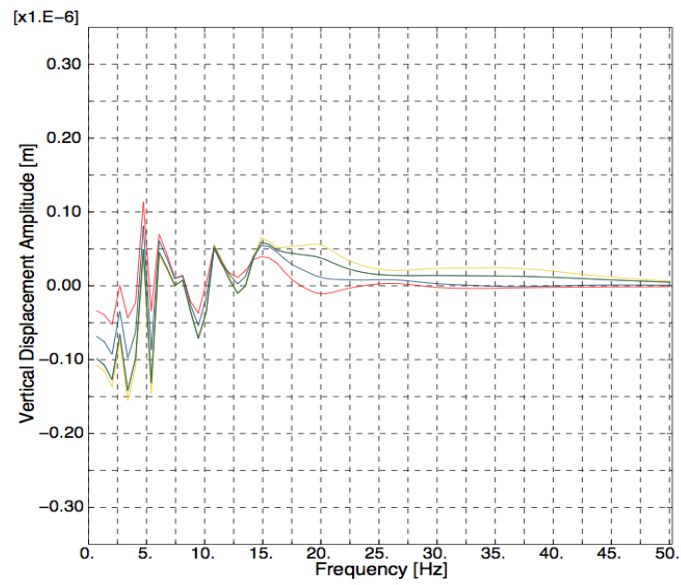
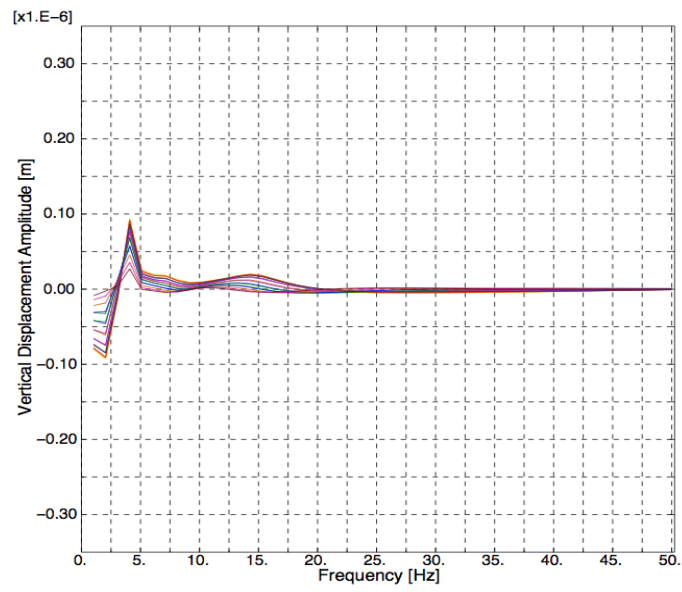Figure A.15: Displacement vs frequency, damping ratio of the soil is 2%
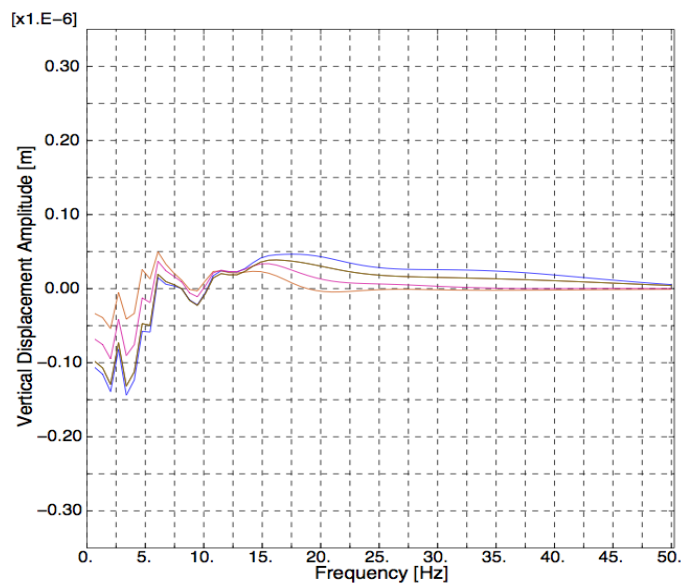
Figure A.16: Displacement vs frequency, damping ratio of the soil is 5%
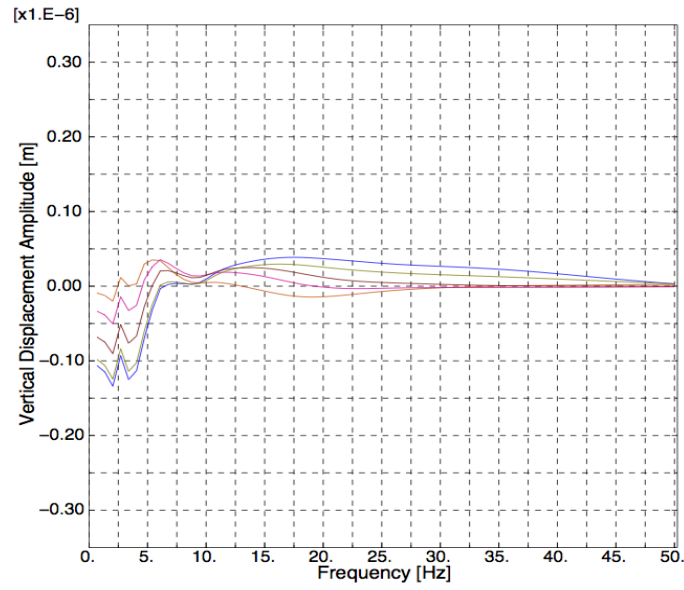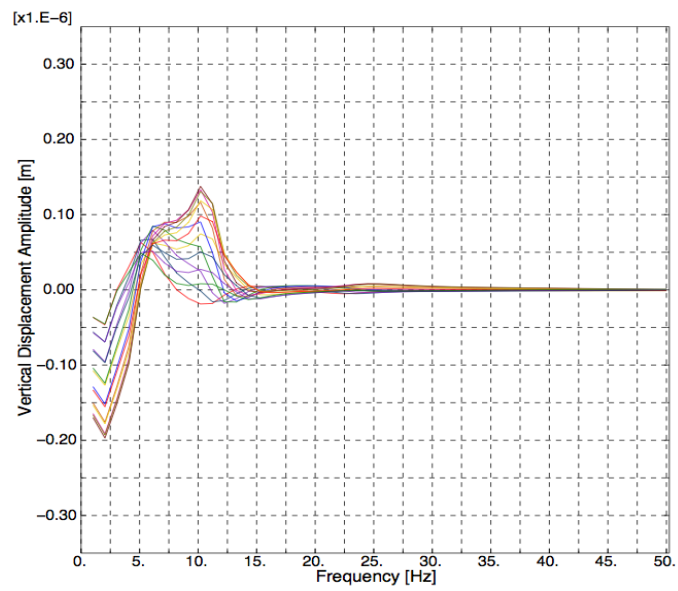
Figure A.17: Displacement vs frequency, damping ratio of the soil is 10%

Figure A.18: Displacement vs frequency, damping ratio of the soil is 20%

Figure A.19: Displacement vs frequency, bus placed on the road

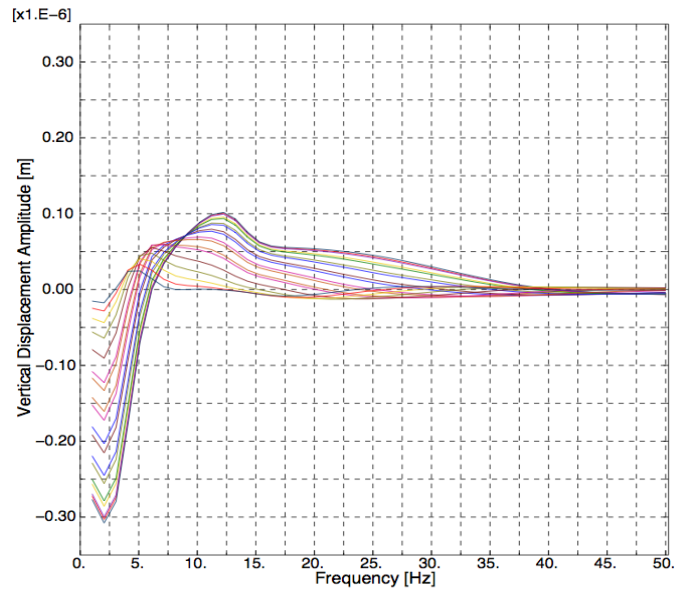Figure A.20: Displacement vs frequency, bus placed on the bridge

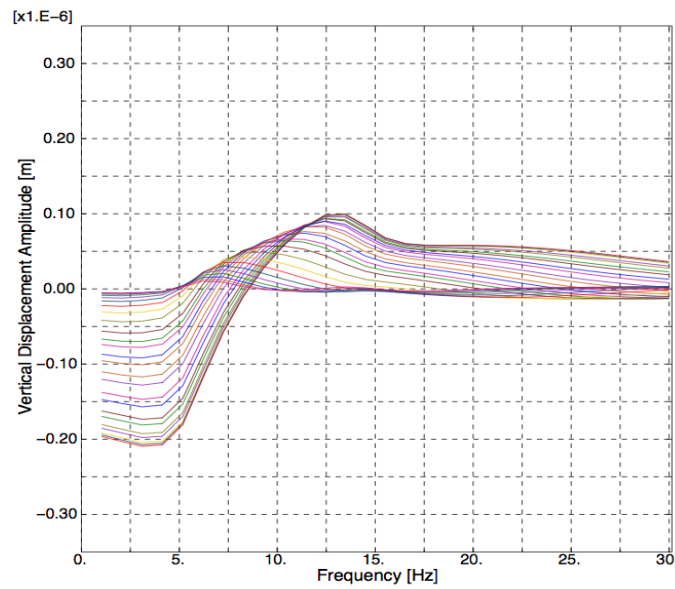Figure A.21: Displacement vs frequency, bus placed on the road and on the bridge

Figure A.22: Displacement vs frequency, bedrock, bus placed on the road and on the bridge
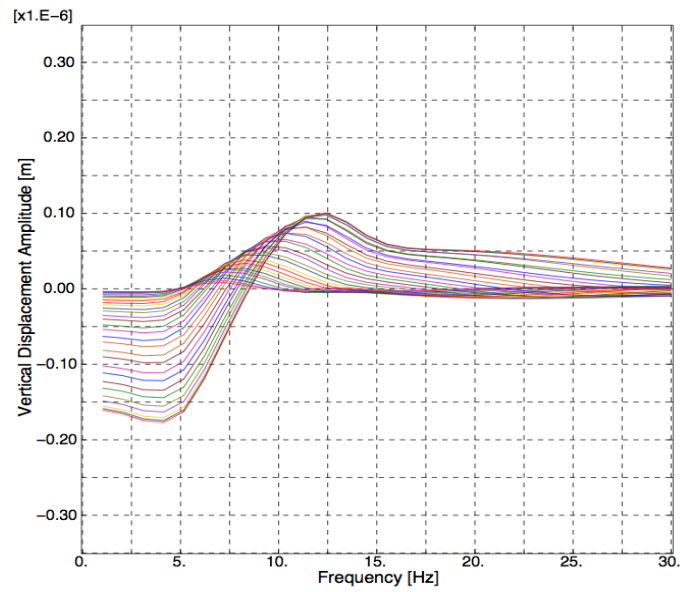
Figure A.23: Displacement vs frequency, bedrock, 1 pillar, bus placed on the road and on the bridge
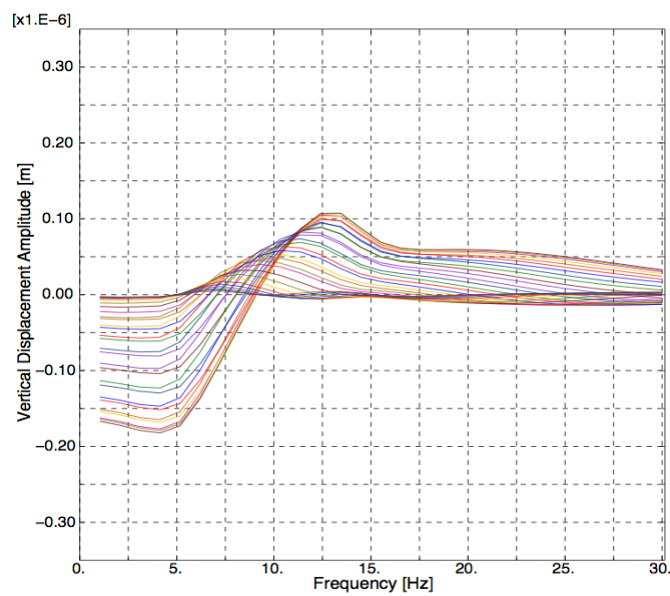

Figure A.24: Displacement vs frequency, bedrock, 2 pillars, bus placed on the road and on the bridge
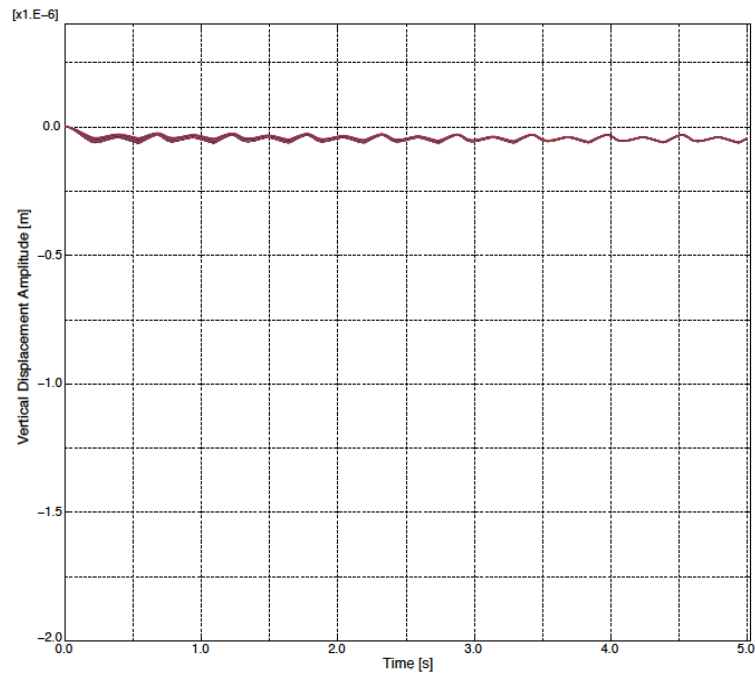
A.2. Figures Transient Analyses

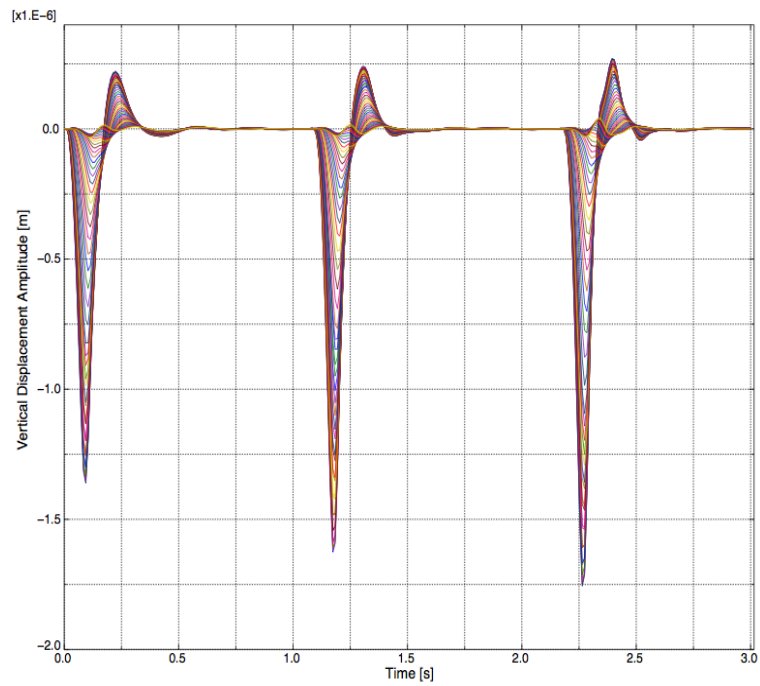Figure A.25: Displacement vs frequency, walking load

Figure A.26: Displacement vs frequency, road irregularities

B. Appendix

B.1. Damping Ratio: Matlab code

```
function rayleigh
close all
format compact
format short

    %———Soil=0.20
% w1=6;
% w2=20;
% zeta=0.2;

    %———Soil=0.10
% w1=6;
% w2=20;
% zeta=0.10;

    %———Soil=0.05
% w1=6;
% w2=20;
% zeta=0.05;

    %———Soil=0.02
% w1=6;
% w2=20;
% zeta=0.02;

    %———Soil=0.01
w1=6;
w2=20;
zeta=0.01;

alpha=zeta*2*w1*w2/(w1+w2)
beta=zeta*2/(w1+w2)
```

```
    %————————alpha:
%Soil20=1.8;
%Soil10=0.94;
%Soil5=0.46;
%Soil2=0.18;
%Soil1=0.092;

    %————————beta:
%Soil20=0.015;
%Soil10=0.0077;
%Soil5=0.0038;
%Soil2=0.0015;
%Soil1=0.00077;

wn=linspace(0,30,30);
for i=1:30
    zetan(i)=alpha/(2*wn(i))+beta*wn(i)/2;
end

y=linspace(0,5*zeta,30);

plot(wn,zetan)
XLABEL('Frequency [Hz]')
title('Rayleigh damping Soil')
YLABEL('Damping ratio')
hold on
plot(wn,1.15*zeta,'r.')
plot(wn,zeta)
plot(wn,0.85*zeta,'r.')
plot(5,y,'r.')
plot(25,y,'r.')
```

B.2. RMS: Matlab code

```
clear all
format short

dt=0.0097; %Type in manually.
dt=analysis time/number of steps ;
T=1; %Always 1 s according to MAX-lab
d=[introduce the values of the vertical displacement amplitudes from Abaqus];
```

```
nofips=floor(1/dt);

for i=1:length(d)-(nofips-1)
    D=d(i:i+(nofips-1)).^ 2;
    Dsum=sum(D);
    Drms(i)=sqrt(Dsum*dt/T);
end
Drms;
max_rms=max(Drms)
```

Bibliography

[1] Anil K. Chopra (1995). *Dynamics of structures.* Prentice Hall

[2] Ottosen N. S. and Petersson H. (1992). *Introduction to the finite element method.* Prentice Hall

[3] Zienkiewicz O.C. and Taylor R.L. *The Finite Element Method*, Butterworth-Heinemann (5th edition. 2000). Vol.2

[4] Austrell, Per-Erik, 2010: *Lecture notes: Dynamics of structures.* Division of Structural Mechanics

[5] Avello Iturriagagoitia, Alejo, 2010: *Lecture notes: Teoría de máquinas.* Universidad de Navarra.

[6] O. Hunaidi, W. Guan and J. Nicks (2000): *Building vibrations and dynamic pavement loads induced by transit buses.* National Research Council Canada.

[7] Bard Delphine, Persson Kent & Sandberg Göran (2008). *Human footsteps induced floor vibration.* Acoustics'08, Paris France, July 2008.

[8] SIMULIA (2008). *Abaqus manual 6.9: Getting started with Abaqus*

[9] Lievens, Matthias & Brunskog, Jonas (2007). *Model of a person walking as a structure borne sound source.* International congress on acoustics. Madrid (september 2007)

[10] Pavic, Aleksandar & Reynolds, Paul (2002). *Vibration serviceability of Long-Span concrete building floors (parts 1 and 2).* The shock and vibration digest.

[11] White, Glen. *Introducción al análisis de vibraciones.* Azima DLI.

[12] Heyden Susanne, Dahlblom Ola, Olsson Anders & Sandberg Göran. (2007). *Indroduktion till Strukturmekaniken.* KFS i Lund AB

[13] MAX-lab, Lunds Universitet. *http://www.maxlab.lu.se/.* November 17th 2009.

[14] SWECO AB. (2009). *Drawings MAX-IV.*

[15] Blyth F.G.H. & de Freitas M.H. (1984). *A Geology for Engineers.* Edward Arnold (7th edition).

[16] Hugo Bachmann, Walter J. Ammann, Florian Deischl (1995); *Vibration problems in structures: practical guidelines*. Birkhauser.

[17] Visual Dictionary online. *http://visual.merriam-webster.com/*. January 15th 2010.

[18] Axelsson Kennet (2005). *Introduktion till GEOTEKNIKEN*. Instutitionen för Geovetenskaper. Uppsala Universitet.

[19] *Encyclopedia Britannica*. Volume V04, Page 320 of the 1911.

[20] Ohlrich M, Hugin C.T. (2003). *On the influence of boundary constrains and angled baffle arrangements on sound radiation from rectangular plates*. Journal of Sound and Vibration. Volume 277, 6 October 2004.